UNIVERSITY OF VICTORIA

CENTRE FOR EARTH AND OCEAN RESEARCH (CEOR)

Turbulence Measurements with a Moored Instrument

by:

R.G. Lueck, D. Huang, D. Newman and J. Box

CEOR Report: 96-1

March 1996

Postal Address:

University of Victoria
P.O. Box 1700
Victoria, British Columbia
Canada V8W 2Y2

Tel: (604) 721-8848
Fax: (604) 721-6200

DISCLAIMER NOTICE

UNCLASSIFIED

Technical Report
distributed by

DEFENSE
TECHNICAL
INFORMATION
CENTER

DTIC/ Acquiring Information—
Imparting Knowledge

Cameron Station
Alexandria, Virginia 22304-6145

UNCLASSIFIED

THIS DOCUMENT IS BEST
QUALITY AVAILABLE. THE
COPY FURNISHED TO DTIC
CONTAINED A SIGNIFICANT
NUMBER OF PAGES WHICH DO
NOT REPRODUCE LEGIBLY.

Turbulence Measurements with a Moored Instrument

by:

R.G. Lueck, D. Huang, D. Newman and J. Box

CEOR Report: 96-1

March 1996

19960422 017

Turbulence Measurement with a Moored Instrument

by

R.G. Lueck, D. Huang, D. Newman and J. Box

School of Earth and Ocean Sciences, University of Victoria, P.O. Box 1700, Victoria, B.C.,
V8W 2Y2, Canada

Abstract

A new, autonomous and moored microstructure measuring instrument has been tested in coastal waters. The instrument measures shear in the dissipation range of the wavenumber spectrum using 4 shear probes, temperature fluctuations using two FP-07 thermistors, temperature and salinity using three pairs of Seabird sensors, horizontal currents using 2 ducted rotors and a fluxgate compass, and body motions using three accelerometers and a pressure transducer. Data are sampled for 128 seconds every 5 minutes and reduced into ensemble and band-averaged spectra and statistical parameters. The processed data are transferred to a disk every 6 hours along with one 128-second set of unprocessed data. In a two-day experiment, the instrument experienced peak flows of 0.15 m s^{-1} and resolved dissipation rates in currents as slow as 0.03 m s^{-1}. Spectra of velocity fluctuations agree closely with the Nasmyth universal spectrum (Oakey 1982). For dissipation rates, the lower limit of detection is determined by electronic noise while the upper limit is set by the angle of attack of cross-stream velocity fluctuations. Both constraints become less restrictive with increasing current. The electronic noise falls below 10^{-10} W kg^{-1} in flows faster than 0.1 m s^{-1} for which we detected dissipation rates as low as 4×10^{-10} W kg^{-1}. The autonomous instrument makes it possible to obtain long time series at much reduced cost compared to conventional profiling from a ship.

1. Introduction

Oceanic turbulence measurements have been taken for more than 30 years since pioneering work by Grant et al (1962). In the open ocean and away from boundaries turbulence is usually assessed by measuring velocity fluctuations at dissipation scales (0.01 to 1 m) using shear probes (Osborn and Crawford 1980) while temperature fluctuations are measured with thermistors (Gregg 1980) or platinum film thermometers (Oakey 1982). Two types of instruments are currently used to measure oceanic turbulence: (*i*) freely falling profilers to detect horizontal velocity fluctuations and their shear (u, v, $\partial u/\partial z$, $\partial v/\partial z$) along with temperature fluctuations and their vertical gradient (T, $\partial T/\partial z$) and (*ii*) horizontally moving vehicles such as towed bodies (Grant et al 1962; Lueck 1987) and submarines (Osborn and Lueck 1985; Gargett et al 1984) to detect horizontal and vertical velocity fluctuations and their horizontal gradients (v, w, $\partial v/\partial x$, $\partial w/\partial x$) and temperature fluctuations and their horizontal gradient (T, $\partial T/\partial x$).

Conventional profilers, whether horizontal or vertical, are fairly labor intensive and require highly trained personnel as well as dedicated ship operations. Therefore, it is financially and logistically impossible to obtain long time series with conventional profilers. The longest continuous time series taken with conventional profilers lasted 30 days and was extended to 90 days by alternating ships and scientific personnel (Moum et al 1995). It cost over one million dollars for ship time alone. The volume of data collected by microstructure instruments is large, about 500 points per meter per signal, and these data require extensive processing that extends well beyond the duration of the cruise.

A new, moored instrument system has been developed for taking unattended microstructure observations for intervals as long as two months. Using conventional sensors, the instrument *TAMI* (*T*ethered *A*utonomous *M*icrostructure *I*nstrument) measures velocity and

temperature fluctuations at dissipation scales, horizontal currents and the local vertical

gradients of temperature and salinity. These data are processed internally into spectra and

statistics and recorded on a hard disk. While conventional instruments actively travel through

the ocean to profile the slowly evolving turbulent eddies, *TAMI* relies upon ambient currents to

advect such eddies past its sensors, similar to boundary layer measurements (McPhee 1994).

We report here the results from a test mooring of *TAMI* in near-shore waters with weak

tidal currents where flow speeds are similar to open ocean conditions. Our design objectives

and the physical features of the instrument are described next in the section 2. The

deployment, recovery and salient features of the test site are described in section 3. The

collected data and an assessment of the performance of *TAMI* is presented in sections 4 and 5,

respectively. The results of this test are summarized in section 6.

2. Instrument

a. Objectives

Our prime objective was to develop an autonomous instrument capable of measuring shear at microscales (0.01 to 1 m) for the estimation of the rate of dissipation of turbulent kinetic energy. The level of naturally occurring turbulence in the open ocean and away from boundaries is very small and dissipation rates range from about 1 to 1000×10^{-10} W kg^{-1} (Gargett and Holloway 1984) — smaller by several orders of magnitude than found in boundary layers (Johnson et al 1994). The best conventional profilers can detect dissipation rates a little smaller than 1×10^{-10} W kg^{-1} and reaching this level was our goal in the design of *TAMI*. However, useful work can be done with an instrument of 10 times poorer resolution (Dewey and Crawford 1988).

The only practical sensor for resolving microstructure shear is the shear or airfoil probe (Osborn and Crawford 1980). The output of the shear probe is proportional to the cross-stream velocity times the axial velocity when the angle of attack is less than 20°. In practice, the angle of attack is kept small by moving the sensor through the water at speeds large compared to the turbulent fluctuations which are typically 0.01 m s^{-1}. If the motion of the sensor is steady and known over scales of 1 m and shorter, the shear probe reports the cross-stream velocity fluctuations. The shear is obtained by applying the Taylor frozen field assumption. For example,

$$E_p = 2\sqrt{2}\,SUw$$

$$E_s = \frac{\partial E_p}{\partial t} = 2\sqrt{2}\,S\,U^2\,\frac{\partial w}{\partial x} \tag{1}$$

where U is the horizontal speed of the shear probe, w the vertical (cross-stream) velocity, S the sensitivity of the shear probe, E_p the voltage output of the shear probe, E_S the output of an analog differentiator and the numeric factor is an artifact of the method of calibration. All else in (1) being constant, the shear signal reported by the probe is proportional to U^2 while the estimated rate of dissipation

$$\epsilon = \frac{15}{2}\nu\overline{\left(\frac{\partial w}{\partial x}\right)^2} \tag{2}$$

(Fleury and Lueck 1991) is proportional to U^4, where ν is the kinematic molecular viscosity and the over bar denotes a spatial average. The speed of conventional profilers ranges from 0.5 m s^{-1} (Gregg 1987) to 2.7 m s^{-1} (Lueck and Osborn 1985). The speed of the water passing *TAMI* is determined by ambient currents which are typically only 0.1 m s^{-1} (Kunze and Sanford 1984) which renders the reported shear signal 100 times smaller than on a conventional instrument. Although the low sensitivity is a severe challenge, the limitation of all conventional instruments is mechanical vibrations rather than electronic noise (Moum and Lueck 1985). We considered a resolution goal of 1×10^{-10} W kg^{-1} feasible because mechanical vibrations should be very small at low speeds while the noise level of commercially available electronics has continually decreased with time.

Our second objective was to measure temperature microstructure, but not necessarily with sufficient resolution to resolve the rate of dissipation of temperature variance. Because the ocean is thermally stratified, turbulent velocity fluctuations are always accompanied by temperature microstructure and their conjunction confirms the presence of turbulence. Temperature microstructure without velocity signals indicates salt fingering activity (Fluery and Lueck 1991). The microstructure thermometer, which is mounted in close proximity to the

shear probes, will permit the distinction between mixing driven by turbulence and mixing by double diffusion.

Our third objective was to make concurrent fine-scale measurements useful for the interpretation of ocean turbulence and double diffusion. These fine-scale measurements include temperature and salinity and their gradients with *CTD* quality to determine the local internal wave strain, the buoyancy frequency, density ratio and current. The local fine-scale shear was to be measured with an upward looking acoustic doppler current profiler positioned 15 m below *TAMI*. The two instruments have not yet been deployed together.

Our fourth objective was to process the data before recording them in order to greatly reduce both its volume and its post-recovery processing. This processing, however, should leave a reasonable amount of diagnostic information to help assess the quality of the data and the performance of the sensors.

Our fifth objective was to make these measurements unattended for intervals of up to 6 months.

b. Mechanical features

The major mechanical requirement of the instrument is that its sensors point into the flow regardless of the direction of the ambient current and that the instrument provides a stable platform free of vibrations over the time scale of the dissipation estimates. Because many of the requirements for a moored instrument are similar to those of a towed vehicle, we decided to adapt the configuration of Lueck (1987). The main body is a wing tank which is 5 m long and 0.6 m diameter at mid body (figure 1). A sailboat mast 3.5 m long is mounted vertically through the center of the body. A ball-bearing and oil-sealed swivel on the line attached to the bottom of the mast permits the instrument to rotate in response to changes in the direction of

the ambient current. Two vertical fins at the rear provide the torque for rotation. The mast permits a 3.5 m vertical separation of two pairs of Seabird temperature and conductivity sensors. Being rigidly attached to the main body, these sensors also point into the flow for good flushing of the conductivity cells and minimal flow disturbance. A third pair of Seabird sensors is attached at mid body. This triplet of sensor pairs provides measurements of salinity, temperature, density and their vertical gradients as well as measurements of buoyancy frequency and density ratio. The speed of the ambient current is measured by two rotor current meters (McPhee 1992) attached to the upper and lower half of the mast.

A pressure case, 1.5 m long and 0.2 m diameter, houses the electronics and is mounted in the forward half of the vehicle. Four shear probes and 2 FP07 thermistors are mounted on a conical end cap attached to the front of this pressure case. Within the conical end cap are three orthogonal accelerometers and a flux-gate compass. A pressure transducer is attached to the rear end cap. Signals from the Seabird sensors and the rotor current meters enter the instrument through the rear end cap. A second pressure case containing batteries is mounted in the aft half of the body. The dimensions of fore and aft cases are identical and the aft case has flat end caps.

A guard ring with a tear-drop cross-section is attached to the front of the body to protect the turbulence sensors without restricting the flow past these sensors. Two horizontal fins at the rear stabilize pitching motions.

Sensor	Signal	Sampling rate $[s^{-1}]$	Location
Shear Probe	$\partial v_1/\partial x$, $\partial v_2/\partial x$	128	Nose cone (exterior)
	v_1, v_2	16	
Shear Probe	$\partial w_1/\partial x$, $\partial w_2/\partial x$	128	
	w_1, w_2	16	
FP-07 Thermistor	$\partial T_1/\partial x$, $\partial T_2/\partial x$	128	
	T_1, T_2	16	
Accelerometer	a_x, a_y, a_z	128	Nose cone (interior)
Seabird Thermometer	T_{SB1}, T_{SB2}, T_{SB3}	2	1 = top of mast 2 = mid-body 3 = bottom of mast
Cell	C_{SB1}, C_{SB2}, C_{SB3}	2	
Rotor	U_1, U_2	*	1 = upper mast 2 = lower mast
Pressure	P	2	rear end cap of front pressure case.
Compass	θ	*	Nose cone (interior)

Table 1.　　Sensors, location and sampling rate. The rotor pulses are summed for 128 seconds, while the compass is read at the start and end of the data cycle.

We were concerned that high-frequency vibrations from various body appendages and from the mooring line might contaminate the velocity signal sensed by the shear probes. To dampen vibrations, the entire length and circumference of the front pressure case is enclosed in 0.025 m of open-cell polyurethane foam. The notion is that the foam acts as a spring

suspending the case while oscillatory motions of the water in the foam are retarded by viscosity. A plate, which is attached to the rear end cap and which is covered on both faces with foam, prevents the case from sliding fore or aft by more than 0.05 m. Thus, the front pressure case is securely held in the instrument without the use of bolts or clamps. Body vibrations can only be transmitted to the pressure case through the polyurethane foam and through the electrical cables attached to the rear end cap. The rear pressure case is mounted rigidly with bolts.

The cavity for the front pressure cases is made from a thin-wall tube that is welded to the skin of the body at the front and to an interior stiffening rings near mid-body. A similar cavity holds the rear pressure case. The front and rear tubes provide a smooth surface for inserting and retracting the pressure cases. The outside surfaces of these tubes together with the skin of the body provide a cavity of considerable volume. This cavity is filled with syntactic foam and fiberglass balls for buoyancy. Buoyancy and weight can also be attached inside the tail section for trimming the pitch of the body.

In air, the instrument weighs 4500 Nt. In water, it is buoyant by 550 Nt. There is about 120 liters of floodable volume inside the instrument, so its enclosed mass underwater is 570 kg. The effective mass, real and entrained mass, is then approximately 1000 kg which gives the instrument considerable inertia for suppressing high-frequency vibrations.

With only 550 Nt of buoyancy the instrument cannot be moored from a very long line. Indeed, it was not our intention to use the instrument as the main buoyancy element in a mooring, although we did anticipate 900 Nt of buoyancy which we failed to reach because a poor choice of material. In a normal deep water deployment, the mooring line and release are held taught by a 1.4 m diameter syntactic sphere which provides 6200 Nt of buoyancy. This sphere also houses an upward looking acoustic Doppler current profiler (ADCP) (figure 2).

The main instrument is 10 — 15 m above the sphere and only needs to suspend a line of that length less 1.5 m, because of the mast. The ADCP provides a measure of the shear around the instrument for estimates of the Richardson number and a redundant estimate of the current. A standard anchor and acoustic release is attached to the bottom of the mooring and experience has shown that it is wise to place a release between the sphere and the instrument. The buoyancy of the sphere is very large and it can overtake and collide with the instrument upon release of the anchor.

c. Electronics

The major issues in the design of the electronics of *TAMI* were (*i*) the acquisition of data from 19 sensors of varying bandwidth, (*ii*) the *in situ* processing of these data, (*iii*) the storage of data and (*iv*) the power consumption of the electronics.

The rate of sampling of the shear probes and thermistors is determined by the smallest spatial scale that must be resolved for dissipation estimates (2), the speed at which the turbulent eddies are advected past the sensors and the effectiveness of our anti-aliasing filter. Ninety percent of the shear variance resides at cyclic wavenumbers smaller than $0.1k_s$ where

$$k_s = \left(\frac{\epsilon}{\nu^3} \right)^{1/4} \tag{3}$$

is the Kolmogorov wavenumber. Taking $\nu = 1 \times 10^{-6}$ m^2 s^{-1} and an upper limit of dissipation of $\epsilon = 1 \times 10^{-6}$ W kg^{-1} gives an upper wavenumber of 100 cpm which the shear probes can resolve with a small amount of correction (Ninnis 1984). Taking the fastest speed of flow to be 0.3 m s^{-1} gives 30 Hz for the upper limit of resolution. We were not able to find low-power elliptic low-pass filters for anti-aliasing and, instead, made our own 12-pole Butterworth low-pass filter with a cutoff frequency of 43 Hz. Thus, the sampling rate is set to 128 samples per

second and the data are over-sampled in all but the fastest flows. Besides indicating pitch and roll, the accelerometers also measure body vibrations near the shear probes, so these signals are also sampled at 128 per second (table 1). Other signals do not need to be sampled this quickly. The undifferentiated shear probe and thermistors signals are sampled at 16 per second with the intention of using these data to estimate heat fluxes by the covariance method (Fleury and Lueck 1994; Yamazaki and Osborn 1993; Moum 1990). The Seabird temperature and conductivity and the pressure signals are sampled at a rate of 2 per second.

If the data are not processed and simply stored, then they will accumulate at the rate of 1300 samples per second to a total of 3.3×10^9 samples after 1 month. Clearly, the data must be processed *in situ* but this is potentially dangerous because it completely obscures the original time series and quality control may be impossible. The spectrum gives considerable information on the quality of the data. For example, the form of the spectrum can be compared to the empirical universal spectrum after Nasmyth (Oakey 1982). The spectrum reveals narrow band vibrations and the frequency distribution of noise. The signal-to-noise ratio of dissipation estimates can be optimized by integrating the shear spectrum only over the range of wavenumbers where the signal exceeds the noise. The volume of data can be further reduced by ensemble averaging many spectra and by smoothing with frequency. Estimates do not need to be made without interruption. The highest frequency of variability of turbulence statistics, such as dissipation rate and the variance of temperature and salinity, will be the buoyancy frequency which rarely exceeds 6 cycles per hour.

Thus, we implemented a burst sampling strategy. The acquisition and processing goes through the following cycle every 5 minutes: (*i*) a watchdog timer wakes the computer which goes through house keeping chores and energizes those circuits that do not need continuous power, (*ii*) the compass is read and counting of pulses from the current meter rotors begins, (*iii*) all other channels are read for 128 seconds at the rates indicated in table 1, (*iv*) the

compass is read again to check for rotation and rotor counting is terminated, (*v*) data

processing begins, (*vi*) data are stored in nonvolatile memory, and (*vii*) the instrument goes to

sleep. After six hours of these cycles, (*i*) the processed data are transferred from memory to a

hard disk and (*ii*) the unprocessed data from the last cycle are also stored to disk. Thus, four

unprocessed data cycles are available daily. Six hours of processed data contains 210KBytes

while a single cycle of unprocessed data contains 320KBytes. Unprocessed data would have

accumulated to 22.5Mbytes after six hours. The net reduction factor is 43.

Sampled signal	Processing	Type
$\partial v/\partial x$, $\partial w/\partial x$, $\partial T/\partial x$, a_x, a_y, a_z	Spectra and co-spectra for $\partial T/\partial x$ only	I
v, w, T	spectra	II
w, T	co-spectra	III
T_{SB}, C_{SB}	min, max, mean, std	IV

Table 2.   Signal types and their processing.

The data fall into four types (table 2) for the purpose of *in situ* processing. The fast

channels — turbulent shears, temperature gradients and accelerations (Type I, table 2) — are

converted to spectra by the fast fourier transform (FFT) of 32 seconds of non overlapping

data. Four periodograms are ensemble averaged into a single spectrum. These spectra are then

band-averaged in geometrically increasing steps so that the frequency of the spectral points are

nearly uniformly spaced in the logarithm of frequency (table 3). Each spectrum contains 21

points ranging in frequency from 0.0315 to 56.0 Hz. The real part of the cross-spectrum (co-

spectrum) of the two temperature gradients is also calculated because it can be used to

estimated the spectrum of the vertical temperature gradient if the two sensors are on a vertical

line (Fleury and Lueck 1992). In addition to spectra, the statistics of mean, maximum and

minimum are also calculated because they can be used to detect spurious signals such as

plankton hits on the shear probes (Moum and Lueck 1985) and signal saturation, which render

the spectral estimate invalid.

For the medium speed channels — velocity and temperature fluctuations (Type II, table

2) — spectra are estimated from a single FFT of the entire 128 seconds of data and then band-

averaged in a geometric progression of 19 points ranging from 0.008 to 7.0 Hz (table 3). Co-

spectra are calculated for all four combinations of vertical velocity and temperature

fluctuations for making estimates of the vertical flux of heat (Type III, table 2) and these co-

spectra also span from 0.008 to 7.0 Hz.

Only statistics are calculated for the slow channels — Seabird temperature and

conductivity signals and the pressure signal (Type IV, table 2). These statistics consist of the

mean, minimum, maximum and sample standard deviation and a second calculation without

those points that are more than 4 standard deviations from the mean. The compass and rotor

readings are left unprocessed.

Power consumption is a critical issue for any autonomous instrument. Much effort was

made to reduce the power consumption without compromising the objectives of the instrument.

We chose a Low Power Acquisition Control Storage System (LOPACS 1989) because it is a

CMOS based IBM-PC (8086) compatible system with two back-plane slots that can be

energized under software control. Being IBM-PC compatible, a wide variety of software and

hardware is available for the system. The disk drive controller and the digital signal processor

(DSP) are placed into the two slots that can be energized by software and this greatly reduced

the average power consumption. The disk controller is needed only every six hours for less

than 60 seconds while the DSP is energized for only 5 seconds during each 5 minute data cycle. All processing is done by the DSP in 3.5 seconds.

	Type I Data			Type II & III Data	
Bin	f [Hz]	Δf [Hz]	Bin	f [Hz]	Δf [Hz]
1	0.032	0.031	1	0.008	0.008
2	0.063	0.031	2	0.016	0.008
3	0.094	0.031	3	0.024	0.007
4	0.14	0.063	4	0.035	0.016
5	0.20	0.062	5	0.051	0.016
6	0.30	0.125	6	0.075	0.031
7	0.42	0.125	7	0.105	0.031
8	0.61	0.25	8	0.15	0.063
9	0.86	0.25	9	0.22	0.062
10	1.2	0.5	10	0.31	0.125
11	1.7	0.5	11	0.43	0.125
12	2.5	1	12	0.62	0.25
13	3.5	1	13	0.87	0.25
14	5.0	2	14	1.25	0.5
15	7.0	2	15	1.75	0.5
16	10	4	16	2.5	1
17	14	4	17	3.5	1
18	20	8	18	5.0	2
19	28	8	19	7.0	2
20	40	16			
21	56	16			

Table 3.   Frequency distribution of spectral estimates of *in situ* processing. *f* is the center

While the digital electronics can usually be de-energized when not needed without any detrimental effects, this is seldom true for the analog components. An exception are the Seabird thermometers and conductivity cells which are specified to have a 3 second warm up and appear to meet that claim. Because all other analog electronics have long power-up transients they remain energized throughout the entire deployment, and we use micro-power operational amplifiers wherever possible. However, micro-power chips do not meet the noise, impedance and bandwidth requirements for neither the shear probe and thermistor circuits nor the anti-aliasing low-pass filters. We, therefore, use regular op-amps for these parts of the circuitry.

The battery pack consists of 12 piles providing 12 different power rails to the instrument. The majority of the consumption is for the analog signal conditioning (± 7 volts nominal at 0.11 amps) which is on continuously and for the main digital electronics ($+7$ volts nominal at 0.14 amps) which has a duty cycle of 53%. The battery pack can contain up to 318 D-cells which can enrgize the instrument for 30 days if the cells are made of alkaline and 60 days if they are made of lithium. Some cells will always have to be made of alkaline to satisfy the power surges of the disk drive and the DSP but the energy required for these two components is small. We estimate that the duration of deployment could be doubled when it becomes possible to replace the analog circuits with lower power integrated circuits. However, alternate or additional energy sources are required for deployments longer than 60 days.

3. Deployment

The moored instrument *TAMI* was deployed in Satellite Channel at 1500 PST on February 17, 1994 and recovered 59 hours later. It was anchored near the 80 m isobath (figure 3). The method of deployment is similar to other moorings. *TAMI* is lowered into the water first, followed by the floatation sphere. The remainder of the mooring line is then paid

out under tension while the ship sails at about 2 knots until only the anchor is aboard the ship. If no knots or tangles are noticed, the anchor is pushed overboard at the desired location. The main instrument is not directly behind the ship but moves slightly athwartships due to hydrodynamic lift on its tail fins. The mooring of February 1994 was configured with a cement anchor (19000 Nt in air), 2 acoustic releases and a 50 m long and rubber coated 0.0064 m steel cable reaching to the bottom of the floatation sphere. No ADCP was mounted in the sphere. A second rubber coated cable 7 meters long connected the top of the sphere to a swivel attached to the bottom of the mast. *TAMI* was 62 m above the bottom and 18 m below the surface, on average.

Satellite Channel is oriented northwest and forms a minor side passage connecting the Georgia Strait basin with the Pacific Ocean. The southeastern end of Satellite Channel connects with Haro Strait which is the main conduit for exchange with the ocean. The Cowichan river provides a small flow of fresh water into the channel while Sansum Narrows to the north is a very turbulent passage. Tidal currents in Satellite Channel are usually weak and seldom exceed 0.5 m s^{-1}.

4. Observations

a. Heading and current

The alignment of the instrument with the ambient current direction is critical for successful turbulence measurements. We had originally intended to compare the direction readings from *TAMI* against the current deduced by the ADCP in the floatation sphere. The original 1.2 MHz unit proved to be unreliable and was being converted to a 600 kHz unit at the factory during this test in Satellite Channel. We will instead rely on the notion that the current in the channel should be primarily along its axis with significant cross-channel flow only during the change of the tide. The time series of the instrument heading indicates that the

orientation is quite stable for flows exceeding 0.02 m s^{-1} (figure 4a, upper panel). For comparison, a stick diagram of the inferred current, estimated from the mean speed of the upper and lower rotors and heading, is plotted in the lower panel of figure 4a. Both rotors stall at 0.01 m s^{-1} and this condition is indicated by zero flow. Upward pointing sticks indicate flooding (northwest flow) along the axis of the channel, while downward directed sticks represent ebbing. There are discontinuities in the heading around the changing of the tide which indicates an inability of the instrument to align with the flow. Particularly noticeable are tidal reversals with extended periods of speeds under 0.01 m s^{-1}, such as at $t = 39.2$ hr (figure 4b), when the instrument turns by 0.7 cycles in 0.7 hours. The direction stabilizes when the speed exceeds 0.04 m s^{-1}. The orientation of the instrument is more stable for the tidal change at $t = 45.5$ hr (figure 4c) which has only two samples with speeds under 0.01 m s^{-1}. Currents are frequently very weak after $t = 50$ hr (figure 4a) and heading discontinuities are numerous. The progressive vector diagram of the measured current (not shown) indicates that the tidal excursion is 2000 m and 400 m in the along- and cross-channel directions, respectively. Thus, the inferred currents are reasonable and the vertical stabilizer produces enough torque to align *TAMI* into the flow for currents stronger than 0.02 m s^{-1}.

b. CTD

The salinity measured with the three pairs of conductivity cells and thermometers shows the repetitious pattern produced by the tidal advection of horizontal inhomogeneity past the instrument (figure 5). The difference between the three salinity signals reflects the local vertical gradient, which is about 0.06 psu m^{-1}. The salinity gradient is fairly steady except near $t = 25 - 27$ hours when the salinity at the bottom of the mast is almost identical to the salinity at mid-body. Salinity dominates the density variations and the water is almost isothermal. The buoyancy frequency, based upon the density difference between the upper and

lower sensors, is 14 cph with little variation. Thus, the flow speeds are comparable to open ocean conditions but the water in Satellite Channel is far more stratified.

The altitude of the instrument above the bottom is quite steady because the currents are weak and the mooring line (between the anchor and the main float) is extremely tight. The pressure record (figure 4) closely reflects tidal height changes predicted at a nearby reference station.

c. Shear and acceleration time-series

The performance of the moored instrument for measuring turbulent shears is best gauged by examining samples of unprocessed data because such samples are in the same form as provided by conventional instruments. A sample of the shears, $\partial w/\partial x$ and $\partial v/\partial x$, recorded while the mean current speed was 0.145 m s^{-1} (figure 6a), shows intermittent turbulence comparable to the sort of signal reported by a conventional profiler (Gargett et al, 1979, figure 11b). This 128 second long time series is equivalent to a horizontal tow of 18 m and at this speed of 0.145 m s^{-1} the data are over sampled. The temporal variations of variance are more clearly evident when these shears are low-pass filtered at 100 cpm to remove electronic and other noise above the band of interest. The variance of the two components track closely which indicates that the shear probes are measuring turbulence that is close to isotropic.

The temporal variations of variance can be compared against the record of acceleration (figure 6a) to determine if they stem from real environmental signals or are merely an artifact of variations in body vibrations. The vertical acceleration a_z should be compared to $\partial w/\partial x$ and the lateral acceleration a_y to $\partial v/\partial x$ because the shear probes measure relative velocity. If the water is non-turbulent but the probes accelerate then the apparent shears detected by the probes is

$$\frac{\partial}{\partial x}[w, v] = -\frac{1}{U}\frac{\partial}{\partial t}[w, v] = \frac{1}{U}[a_z, a_y] \tag{4}$$

(Moum and Lueck 1985). The three components of acceleration are shown with their full bandwidth and also low-pass filtered at 100 cpm. Clearly, the variation of acceleration are completely uncorrelated with variations of shear. The shear probes are responding to environmental signals.

The accelerometers respond both to inertial accelerations (the signal of interest for judging the quality of the shear probe signals) and to gravity. The pitching and rolling of the instrument will induce a component of gravity along the axis of sensitivity of a_x and a_y, respectively. The signals induced by gravity are

$$[a_x, a_y] = g[\sin(\theta), \sin(\phi)] \tag{5}$$

where θ is the pitch angle (positive with nose up) and ϕ is the roll angle (positive port down). The vertical accelerometer reports mainly inertial acceleration because this sensor is only cosine sensitive to deviations of its axis from vertical. The pitch and roll signals can only be unambiguously separated from the inertial acceleration with rotation sensors which are not carried by *TAMI*. However, the spectral distribution of these two types of signals is different — pitch and roll are dominant at low frequencies while inertial signals are dominant at high frequency. The pitch and roll of *TAMI* can be gauged with the scale on the right side of figure 6a. Typical peak-to-peak variations of pitch are less than 0.1° with a period of 8 s and peak-to-peak roll variations are 0.1° with a period of 20 s. A peak-to-peak roll of 0.03° and 2.5 s period is also evident and this signal may be either roll or inertial acceleration. The pitching motion of conventional vertical profilers is about 1 to 2° after initial transients

disappear (Moum and Lueck 1985; Schmitt et al 1988) and a little larger for towed horizontal profilers (Lueck 1987). Thus, *TAMI* provides and extremely stable platform for the measurement of turbulence at speeds of 0.15 m s^{-1}.

A second sample of unprocessed data taken in a mean flow of 0.045 m s^{-1} is also very similar to data collected with a conventional instrument (figure 6b). At this speed the data span only 6 m, and the turbulence is weak for half of this distance. Again, the variations of variance of the two shears track closely and are uncorrelated with variations of acceleration. The peculiar pulses in the a_y signal are an artifact of the electronics that is absent from the hundreds of other unprocessed records taken since this particular sample. We suspect that the pulses resulted from a poor connection. At this slower speed of 0.045 m s^{-1}, pitch and roll are lower with peak-to-peak amplitudes of 0.03° and there is no roll motion with a period of 2.5 s as occurred at speeds of 0.15 m s^{-1}.

d. Shear and acceleration spectra

Spectra of the shear and acceleration signals shown in figure 6 are estimated using two methods. The continuous lines in figure 7 are the spectra calculated after the instrument was recovered using the unprocessed data. The symbols are the spectra calculated *in situ* by the instrument while in the field. The agreement between the two types of estimates verifies the propriety of the internal data processing of the instrument. The shear spectra have the shape expected for turbulence signals; a slow rise at low wavenumbers to a spectral peak, a rapid descent for wavenumbers larger than the peak and a high frequency rise due to electronic noise. Because the instrument computes spectra rather than total variance, we can integrate the spectra over a limited range of wavenumbers to exclude the parts that are dominated by electronic noise. For the data taken at 0.145 m s^{-1}, the change in slope at 50 cpm (marked by dashed vertical line in figure 7a) identifies the boundary between the range dominated by real

signal and the higher wavenumber range where the spectrum is dominated by noise. The rate

of dissipation, estimated from the variance between 0.2 cpm (the lowest resolved wavenumber)

and 50 cpm, is 1.22×10^{-8} W kg^{-1} and identical (to two decimal places) for both shear probes.

The slope of the spectrum above 50 cpm is considerable flatter for the $\partial w/\partial x$ signal than for

the $\partial v/\partial x$ signal. This is due to the narrow spike in the time series of $\partial w/\partial x$ at $t = 50$ s (figure

6a) which is very likely caused by the collision of that probe with plankton. Three decades

separate the peak of the spectrum of $\partial v/\partial x$ from the trough at 50 cpm which indicates that, at

0.145 m s^{-1}, the instrument has a very favorable signal-to-noise ratio and should be able to

resolve dissipation rates of $O(10^{-10}$ W kg$^{-1})$. The signal resolution of the instrument is

examined further in section 5.b. The signal-to-noise ratio is a little less favorable for the $\partial w/\partial x$

signal because of the spike in the time series.

The spectra of acceleration have been scaled by the square of the flow speed to indicate

the level of signal contamination due to probe motion (4). These scaled acceleration spectra

fall well below the shear probe spectra at wavenumbers larger than 3 cpm, particularly for the

vertical component (figure 7a). At very high wavenumbers, the acceleration spectra are below

the noise level of the shear spectra. Therefore, the resolution of shear is limited by electronic

noise and not probe vibrations which is contrary to the case for conventional profilers (Moum

and Lueck 1985). The acceleration spectra rise above the shear spectra at wavenumbers

smaller than 3 cpm (0.5 Hz) but the output of the accelerometers in this range is dominated by

gravitational signals due to roll and pitch. Roll and pitch have negligible effect on the velocity

signal sensed by the shear probes (Moum and Lueck 1985). The vertical acceleration has a

local peak near 20 cpm (3 Hz) which may contaminate the shear probe spectrum slightly at

lower dissipation rates. Subsequent work indicates that the mast resonates near 3 Hz.

Even at a flow speed of only 0.045 m s^{-1}, the data have favorable spectra (figure 7b).

The resolution of the shear probes is more noticeably limited by electronic noise than at

0.145 m s^{-1} but there are still three decades separating the peak of the shear spectrum from the trough at 150 cpm. The rate of dissipation estimated from the two probes agree well with values of 7.1 and 5.0×10^{-7} W kg^{-1} from the signals of $\partial w/\partial x$ and $\partial v/\partial x$, respectively. The scaled spectra of vertical and lateral accelerations are below the shear spectra at all wavenumbers. Thus, the instrument should resolve dissipation rates down to $O(10^{-9}$ W kg$^{-1})$ at flows of only 0.05 m s^{-1}.

5. Discussion

a. Comparison against the universal spectrum

To test whether the shape and level of the shear spectra conform to the theoretically expected turbulence spectra, we (*i*) convert twelve samples from each probe to velocity spectra, (*ii*) normalize these spectra by the Kolmogorov scaling and (*iii*) compare these spectra against the empirical universal spectrum of Nasmyth (Oakey 1982) in figure 8. The rate of dissipation, required for the normalization, is determined using standard techniques. The variance of the shear is obtained by integrating the shear spectrum from the lowest wavenumber to the wavenumber of the spectral minimum (as shown by the dashed line in figure 7, for example). If the spectral minimum is above 100 cpm, the integral is terminated at 100 cpm. Correcting the spectra for the high wavenumber attenuation by the probe using the calibration of Ninnis (1984) (see, for example, Fleury and Lueck 1994) makes little difference to the estimated variance. The dissipation rate is then determined from (2). No systematic departure of the measured velocity spectra from the universal curve is evident and individual spectral points deviate by less than a factor of 3 (figure 8). Thus, a consistent estimate of dissipation rate is obtained from the variance of the shear and from the spectral level of velocity in the minus-five-thirds inertial subrange.

A more stringent comparison against the universal spectrum of Nasmyth is obtained with the shear spectrum because it spans a smaller range of values than does the velocity spectrum. We have selected 405 spectra using the criteria that (*i*) they come from flows stronger than 0.03 m s^{-1}, (*ii*) the rms angles of attack is smaller than $5°$ (discussed below), (*iii*) the ratio of dissipation estimates from the *w*- and *v*-probes fall within 0.4 and 3.2, (*iv*) the rate of turning of the instrument is less than $3°$ per minute, (*v*) the shear spectra exceed the scaled acceleration spectra for all wavenumbers larger than 3 cpm and (*vi*) the maximum and minimum output of the analog-to-digital converter does not exceed half its full scale. Condition (*vi*) is used to exclude large impacts with plankton. The ensemble average of theses 405 spectra agree very closely with the universal shear spectrum (figure 9) but the universal curve is outside of the 95% confidence limit of the measured spectrum. The spectral peaks differ by 10%. The observed spectrum is higher than the universal one at wavenumber smaller than the peak while the observed spectrum is higher at wavenumber larger than the peak. The area under the two spectra is, of course, identical. Although there are several predictions for the spectrum (Pao 1965; Panchev and Kesich 1969) these analytic expressions contain adjustable parameters that have not been rigorously verified against oceanic observations. A comparison of shear spectra from two billows in a tidal channel by Seim and Gregg (1994) against the Nasmyth and theoretical forms gives an agreement similar to that shown in figure 9.

b. Electronic noise

To estimate the noise level of the instrument we use the spectra of data collected when the speed was less than 0.01 m s^{-1}. Smaller values cannot be distinguished because the rotors stall at this speed. The assumption is that the voltage produced by the shear probes is negligible because the probe's output is proportional to speed squared. However, some signal maybe still be produced by eddy shedding, if the flow is non-zero and the instrument is not aligned with the remnant current. We selected 26 spectra of $\partial w/\partial x$ and 24 spectra of $\partial v/\partial x$ that

have no evidence of spurious signals. There is no systematic difference between the spectra from the two probes. The ensemble average of these 50 spectra defines the noise spectrum for the instrument (figure 10). This spectrum is expressed in counts squared per hertz and should always be present in the integer data samples produced by the analog-to-digital converter. The level of this spectrum in terms of shear depends on the speed and the sensitivity of the probes. Using the calibrated sensitivity of the probes and the gain of the electronics, this noise spectrum can be converted into the shear spectrum produced by electronic noise for any given speed. The lower limit of resolution of the instrument can be deduced by comparing the spectra of electronic noise (in terms of shear) for a variety of speeds against the Nasmyth universal spectrum for a range of dissipation rates (figure 11). We will consider the shear to be resolved if the noise spectrum is at least a factor of 10 below the universal shear spectrum. Thus, at 0.05 m s^{-1} the instrument resolves dissipation rates as small as 1×10^{-9} W kg^{-1} which was deduced from the sample spectrum in figure 7b. At 0.03 m s^{-1}, the resolution is only 1×10^{-8} W kg^{-1} and this should be considered to be the limit of operating speed because oceanic dissipation rates seldom exceed this value below the surface mixing layer (Yamazaki and Lueck 1987; Lueck 1988). At speeds larger than 0.1 m s^{-1} the resolution is better than 1×10^{-10} W kg^{-1} and the performance of the moored instrument is comparable to the best conventional profilers. The deployment in Satellite Channel did not provide any data for speeds greater than 0.15 m s^{-1} so the performance at greater speeds is conjectural. It is safe to assume that the contribution by electronic noise will decrease with increasing speed as shown in figure 11 because this component of the noise is independent of speed. However, mechanical vibrations induced by eddy shedding and other non-steady flows around the instrument at higher speeds will eventually become large (which is the case for conventional profilers) and this component of the noise in the shear probe signal will set the limit of resolution. Subsequent deployment in a fast tidal channel indicate vibrations at several frequencies when the flow exceeds 0.7 m s^{-1}.

c. Angle of attack

The angle of attack must be smaller than about 20° for the shear probes to respond linearly to cross-stream velocity fluctuations (Osborn and Crawford 1980). Our calibrations indicate that the probe sensitivity is typically larger by 24% at angles of 10° compared to zero degrees of attack. The limitation imposed by the angle of attack is seldom a problem with conventional profilers because these instruments move through the water at speeds much faster than the magnitude of the turbulent velocity fluctuations. However, a small angle of attack cannot be guaranteed for a moored instrument when the "mean" speed gets small. Some combinations of speed and turbulence intensity may impose large angles of attack. The instantaneous angle of attack cannot be estimated from the spectra of shear or velocity. The rms angle of attack can be estimated from velocity spectra using two methods. Using the first method, the shear spectra are converted to velocity spectra and the variance of the cross-stream velocity is estimated by spectral integration from the lowest wavenumber of the spectrum (typically 0.3 cpm) up to the lesser of either $k/k_S = 0.3$ or 100 cpm. The range of integration is the same range used for the estimation of dissipation rates. Significant velocity fluctuations may exist at wavenumbers smaller than the lower bound of the shear spectra. Thus, this first method gives a lower bound on the rms cross-stream velocity. With the second method, the estimated dissipation rate is used to infer the velocity spectrum from the Nasmyth universal spectrum over the same wavenumber range used in the first method. Integration of this inferred spectrum gives velocity estimates only slightly larger than obtained with the first method.

For gaussian signals, the peak value is very nearly three times the rms. However, turbulent signals have considerable kurtosis and the ratio of peak-to-rms is larger than 3. We have set 5° as the limit of the rms angle of attack for the acceptance of dissipation estimates. This criterion of 5° is somewhat arbitrary which means that some of the dissipation estimates

will come from time series where the largest instantaneous values are exaggerated. However, the variance will be exaggerated by less than the largest instantaneous shears. Thus, large dissipation values are biased to larger values at low speeds. The estimated rms angle of attack is regressed against speed and dissipation rates in figure 12. Only a few observations exceed 5° and these occur, as expected, for the slowest flows and the largest dissipation rates.

Thus, the resolution of oceanic dissipation by the instrument, at any given speed, is determined by two factors; the lower bound is set by the electronic noise and the upper bound is set by the angle of attack. These constraints are mapped into the ϵU-plane (figure 13) along with the estimated angle of attack to delineate the useful range of the moored instrument. The minimum useable flow is 0.03 m s^{-1} for our criterion of 5° while a more conservative criterion of 3° for the angle of attack dictates that the flow should exceed 0.04 m s^{-1}.

The ability of the shear probe to resolve very small dissipation rates even at speeds of only 0.04 m s^{-1} is a testimony of its extraordinary sensitivity of this device and challenges a commonly held notion that large profiling speeds are required with conventional profilers to make use of the shear probe. This notion is motivated by the U^4 dependence of the dissipation estimates (1,2) but fast profiling frustrates attempts to make simultaneous temperature microstructure measurements because these require slow speeds to utilize the limited frequency response of thermistor temperature sensors. Researchers interested in taking velocity and temperature profiles may be able to take both simultaneously at slow speeds.

d. Shear probes

Two aspects of the shear probes are of concern for long-term deployment — immunity to corruption by moisture and sensitivity at low speeds. It is well known among users of the shear probe that the piezo-ceramic element, which converts the lift force of cross-stream velocity fluctuations into an analog voltage, must be electrically isolated from seawater. For

proper operation the two electrodes on the ceramic must be separated by a resistance of more than 10^{10} ohms. Thus, moisture must be prevented from penetrating to the surface of the ceramic. Test conducted in our laboratory show that the silicon rubber shroud on the tip of the probe blocks moisture for only a few hours at atmospheric pressure. To extend the duration of high resistance, it is common to coat the ceramic with epoxy during manufacture and to shrink polyolefin tubing over the ceramic while the epoxy is still wet. This assemblage is then epoxied into the end of a stainless steel tube. Our tests indicate that the polyolefin tubing blocks the penetration of moisture for several weeks at atmospheric pressure but only for about one day at 300 dBar. The sensitivity of the shear probes using voltage amplifiers drops by more than half when the resistance of the probes decreases below 10^{10} ohms. Others have noticed large pyro-electric effects after several profiles to depths greater than 1000 m (Schmitt 1994, personal communication). A change of sensitivity is difficult to detect at sea other than by comparing a well "soaked" probe against a fresh and "dry" one. We tried to coat the ceramic with teflon and with glass to mitigate the penetration of moisture but, this did not work. However, we found that metal coating did work. In this technique, which requires meticulous attention to details, the polyolefin covered ceramic is epoxied into the stainless steel tube as usual. All exposed epoxy and polyolefin is then coated with a conductive paint. The tip of the probe, including about 0.005 m of the stainless steel tubing is then immersed in a bath and a layer of eutectic solder (37 parts tin to 63 parts lead) is electroplated onto the probe to a thickness of $3 - 5 \times 10^{-6}$ m. Thus, a contiguous layer of metal separates the ceramic from seawater. A standard tip of silicon rubber is then molded on to the probe to give it its final shape. Our test show no measurable moisture penetration after exposure to water at atmospheric pressure for 90 days, that is, the resistance remained above 10^{11} ohms. *TAMI* was deployed for 23 days in 1993 in the Canary basin at a depth of 300 m but failed to work for a number of reasons. However, within an hour of its recovery, the resistance of the shear probes were measured to be 5×10^{10} ohms!

It is commonly held that the sensitivity of the shear probes is independent of speed. As discussed by Osborn and Crawford (1980), the original formulation of the lift force on the probe was derived for aeronautical purposes, that is, for large Reynolds number flows. The total cross-stream force is composed of a pressure force which is proportional to speed squared and viscous drag which is proportional to speed. Pressure forces greatly exceed viscous drag at large Reynolds numbers. By the method of calibration, the value of the sensitivity coefficient in (1) due to pressure is independent of speed while the relative contribution due to viscous forces will increase with decreasing speed. We have extended our calibrations, which are normally made at 0.7 m s^{-1}, down to 0.07 m s^{-1} and find that the sensitivity increases by 25% at the lower speed (figure 14). This speed dependence has been taken into account in all estimates of velocity and shear.

e. Time series of ϵ

To create a time series of the rate of dissipation, we have selected all values that meet the criteria given in section 5.a except for condition (*iii*). Deleting criterion (*iii*) permits us to use, where necessary, estimates from only a single probe. The rate of dissipation varies by more three orders of magnitude but no tidal signature is evident (figure 15, upper panel). The rates are not correlated with speed. The smallest dissipation estimate is 4 times larger than our estimated noise level. The noise spectrum (figure 10) was not subtracted from the measured shear spectrum for the dissipation estimates in figure 15.

The water is highly stratified and the Ozmidov or buoyancy scale, $L_o = (\epsilon/N^3)^{\frac{1}{2}}$ seldom exceeds 0.1 m and is typically only 0.05 m (figure 15, second panel from top). Taking L_o as the typical vertical scale for turbulent eddies, it is clear that the observed dissipation rates are unrelated to local bottom friction. A more likely source for the turbulence are internal waves generated by topographic interaction of the tidal stream at remote locations such

as Sansum narrows to the north of Satellite Channel. The buoyancy Reynolds number, $Re = \epsilon(\nu N^2)^{-1}$, which provides a measure of the ratio of scales suppressed by stratification to those dampened by viscosity, is typically 10 and seldom exceeds 100 (figure 15, third panel from top). With such a small separation of scales it may seem suprising that the spectra of velocity conform well to the empirical universal spectrum of Nasmyth. Gargett et al (1984) found anisotropy between the vertical and horizontal components of velocity fluctuations at buoyancy Reynolds numbers less than 200 in decaying turbulence. However, Yamazaki et al (1990) found that the variances of $\partial w/\partial x$ and $\partial v/\partial x$ can be equal even at buoyancy Reynolds mumbers as small as 20.

d. Experience gained

People interested in developing a moored microstructure instrument may wish to consider some of our frustrations and the current inadequacies of our instrument. The rigidly attached bottom mast causes the instrument to pitch because the instrument can be considered to be towed from a point on the bottom of the mast. The drag force on the body produces a horizontal torque around the bottom of the mast that pitches the nose upward. The rear horizontal stabilizer mitigates the pitch but does not eliminate it. A counter torque is only produced for a non-zero angle of attack against the rear stabilizer. The torque produced by drag and the pitch angle can be greatly reduced by hinging the mast at the bottom of the body, which shortens the moment arm.

The analog-to-digital converter board supplied by the manufacturer of the computer system was specified to be a 16-bit unit but performed only like an ideal 11-bit converter. After a considerable amount of trace cutting and rewiring to make the sampling synchronous with the main computer clock, the bit noise became comparable to an ideal 15-bit converter. The actual converter chip is manufactured by the Crystal Semiconductor Corporation and uses

a charge transfer techniques rather than the more conventional and power hungry technique of voltage division by resistive ladders. A major drawback of the charge transfer technique is that the device momentarily draws a large current on its input at the start of conversion. The multiplexer output is connected directly to the converter input and the resistance of the multiplexer impedes the current draw. The two should be isolated with an operational amplifier of low output impedance. A third problem of unknown origin is that the offset of the analog-to-digital converter has two stable states. The offset remains constant after power is applied but jumps by approximately 11 counts the next time it is energized. This required us to sample a ground reference to correct the data.

Conclusions

A new, autonomous and moored instrument system has been developed for the measurement of the rate of dissipation of kinetic energy using conventional shear probes and for the observation of current, its shear, buoyancy frequency, density ratio, temperature and salinity variations. The instrument carries sufficient batteries to operate for up to one month using alkaline cells and 2 months with lithium cells. This platform addresses the need for long time series at a reduced cost in terms of ship time and personnel. The instrument relies upon ambient currents to advect turbulent eddies past its sensors and, even though such flows are weak compared to typical profiling speeds with conventional instruments, it can operate in flows as slow as 0.03 m s^{-1}. The lower limit of detection of dissipation rates is set by electronic noise while the upper limit is set by the angle of attack of cross-stream velocity fluctuations and both effects become less restrictive with increasing speed of flow. The character of the space series of microstructure shear of unprocessed data are very similar to the series taken with conventional instruments while the spectra of velocity and shear agree closely with the Nasmyth empirical spectrum in both shape and level.

Bibliography

Dewey, R.K., and W.R. Crawford, 1988: Bottom stress estimates from vertical dissipation rate profiles on the continental shelf. *J. Phys. Oceanogr.*, **18**, 1167-1177.

Efron, B. and G. Gong, 1983: A leisurely look at the bootstrap, the jackknife, and cross-validation. *Amer. Statician*, **37**, 36-48.

Fleury, M., and R. G. Lueck, 1992: Flux across a thermohaline interface. *Deep-Sea Res.*, **38**, 745-769.

Fleury, M. and R.G. Lueck, 1991: Microstructure in and around a double-diffusive interface. *J. Phys. Oceanogr.*, **22**, 701-718.

Fleury, M., and R. G. Lueck,1994: Direct heat flux estimates using a towed vehicle. *J. Phys. Oceanogr.*, **24**, 801-818.

Gargett, A.E., and G. Holloway, 1984: Dissipation and diffusivity by internal wave breaking. *J. Mar. Res.* **42**, 15-27

Gargett, A.E., T.B. Sanford and T.R. Osborn, 1979: Surface mixing layers in the Sargasso Sea. *J. Phys. Oceanogr.*, **9**, 1090-1111.

Gargett, A.E., T.R. Osborn and P.W. Nasmyth, 1984: Local isotropy and the decay of turbulence in a stratified fluid. *J. Fluid Mech.* **144**, 231-280.

Grant, H.L.,R. W. Stewart and A. Moilliet, 1962: Turbulence spectra from a tidal channel. *J. Fluid Mech.*, **12**, 241-263.

Gregg, M. C., 1980: Microstructure patches in the thermocline. *J. Phys. Oceanogr.*, **6**, 915-943.

Gregg, M. C., 1987: Diapycnal mixing in the thermocline: a review. *J. Geophys. Res.*, **92**, 5249-5286.

Johnson, G.C., R. G. Lueck and T. B. Sanford, 1994: Stress on the Mediterranean outflow plume: Part II turbulence dissipation and shear measurements. *J. Phys. Oceanogr.*, **24**, 2084-2092.

Kunze, E., and T. B. Sanford, 1984: Observations of near-inertial waves in a front. *J. Phys. Oceanogr.*, **14**, 566-581.

LOPACS, 1989: Low power acquisition control storage system, Star Engineering, Inc., 29 Wall Street, Foxboro, Ma., 02035.

Lueck, R.G., 1987: Microstructure measurements in a thermohaline staircase. *Deep Sea Res.* **34**, 1677-1688.

Lueck, R.G., 1988: Turbulent mixing at the Pacific subtropical front. *J. Phys. Oceanogr.*, **18**, 1761-1774.

Lueck, R.G., and T. Osborn, 1985: Turbulence measurements in a submarine canyon. *Cont. Shelf Res.*, **4**, 681-698.

McPhee, M.G., 1992: Turbulence heat flux in the upper ocean sea ice. *J. Geophys. Res.*, **97**, 5365-5379.

McPhee, M.G., 1994: On the turbulent mixing length in the oceanic boundary layer. *J. Phys. Oceanogr.*, **24**, 2014-2031.

Moum, J.N., 1990: The quest for K_ρ -- Preliminary results from direct measurements of turbulent fluxes in the ocean. *J. Phys. Oceanogr.*, **20**, 1980-1984.

Moum, J., M.C. Gregg, R.C. Lien and M.E. Carr, 1995: Comparison of turbulence kinetic energy dissipation rate estimates from two ocean microstructure profiles. *J. Atmos. Oceanic Technol..*, **12**, 346-366.

Moum, J., and R.G. Lueck, 1985: Causes and implications of noise in oceanic dissipation measurements. *Deep Sea Res.*, **32**, 379-390.

Ninnis, R.M., 1984: The effect os spatial averaging on airfoil probe measurements of oceanic velocity microstructure. Ph.D. dissertation, University of British Columbia, 109pp.

Oakey, N.S., 1982: Determination of the rate of dissipation of turbulence energy from simultaneous temperature and velocity shear microstructure measurements. *J. Phys. Oceanogr.*, **12**, 256-271.

Osborn, T.R. and W.R. Crawford, 1980: An airfoil probe for measuring turbulence velocity fluctuation in water. *Air-Sea Interaction, Instruments and Methods.* F. Dobson, L. Hasse and R. Davis, Eds. Plenum, 801pp.

Osborn, T. R., and R. G. Lueck, 1985: Turbulence measurements from a submarine. *J. Phys. Oceanogr.*, **15**, 1502-1520.

Panchev, S., and Kesich, 1969: Energy spectrum of isotropic turbulence at large wavenumbers. *C.R. Acad. Bulg. Sci.*, **22**, 627-630.

Pao, Y. 1965: Structure of turbulent velocity and scalar fields at large wavenumbers. *Phys. Fluids.*, **8**, 1063-1075.

Schmitt, R.W., J.M. Toole, R. L. Koethler, E.C. Mellinger and K.W. Doherty, 1988: The development of a fine - and microstructure profiler. *J. Atmos. Oceanic Technol..*, **5**, 484-500.

Seim, H.E., and M.C. Gregg, 1994: Detailed observations of a naturally occurring shear instability. *J. Geophys. Res.*, **99**, 10049-10073.

Yamazaki, H., and R.G. Lueck, 1987:Turbulence in the California undercurrent. *J. Phys. Oceanogr.*, **17**, 1378-1396.

Yamazaki, H., and T.R. Osborn, 1993: Direct estimation of heat flux in a seasonal thermocline. *J. Phys. Oceanogr.*, **23**, 503-516.

Yamazaki, H., R.G. Lueck and T.R. Osborn, 1990: A comparison of dissipation measurments from simultaneous horizontal and vertical profiles. *J. Phys. Oceanogr.*, **10**, 1778-1786.

Figure Captions

1.   Sketch of *TAMI* (*T*ethered *A*utonomous *M*icrostructure *I*nstrument) which can be anchored using standard techniques and which measures fluctuations of cross-stream velocity and temperature and their horizontal gradients at microscales using shear probes and thermistors. The vertical gradients of conductivity and temperature are measured with three pairs of Seabird sensors. The speed of flow past the instrument is measured with two ducted rotors on the upper and lower masts. The instrument is 5 m long and has a diameter of 0.6 m.

2.   Typical mooring configuration. The main floatation element is a 1.4 m diameter sphere made of syntactic foam with a buoyancy of 6200 Nt. The line between the acoustic release and the float can be as long as 5000 m. The float also houses and upward looking acoustic doppler current profiler (ADCP). The main instrument, *TAMI*, is 12 m above the float — within the measurement range of the ADCP yet outside the acoustic beams.

3.   The location of the deployment of *TAMI* on February 17-19 of 1994 (asterisk) in Satellite Channel, a minor channel connecting the Georgia Basin to the Pacific Ocean to the east of Juan de Fuca Strait.

4.a   Time series of heading measured every 5 minutes (dots, upper panel) expressed in cycles. The solid line is the expected rotation for the M_2 tide. The lower panel depicts the current vector (sticks) from the measured speed (thin line) and heading, while the thick line is the pressure.

when the flow was weaker than 0.01 m s^{-1} for 40 minutes.

4.c   Close-up of the heading and current during the change of tide around $t = 45.5$ hours when the flow was weaker than 0.01 m s^{-1} for only 10 minutes.

5.   Salinity deduced from the top (T), middle (M) and bottom (M) conductivity and temperature sensors (upper panel) along with the current vectors (lower panel). Rapid variations of salinity occur around the change of the tide.

6.a   Unprocessed time series of the shears $\partial w/\partial x$ and $\partial v/\partial x$ recorded by the instrument with full bandwidth (upper two traces, upper panel) and the same shear low-pass filtered at 100 cpm (lower two traces, upper panel) while the flow was 0.145 m s^{-1}. The concurrent full bandwidth acceleration (upper three traces, lower panel) and the accelerations low-pass filtered at 100 cpm (lower three traces, lower panel). The x-acceleration can also be interpreted as pitch for low frequencies (right hand scale) and the y-acceleration as roll. All traces have been offset for clarity.

6.b   Same as for 6.a but for unprocessed data collected during a flow of only 0.045 m s^{-1}.

7.a   Spectra of the shear in figure 6.a with $\partial w/\partial x$ in the left panel and $\partial v/\partial x$ in the right panel. The corresponding acceleration spectra have been scaled by U^{-2} to indicate the contamination due to body vibrations. For the low frequencies, the spectrum of a_y is mainly roll while the spectrum of a_z has a small contribution from pitch and roll. Pitch and roll do not affect the measured shears. The solid lines are the spectra calculated from the unprocessed data after the instrument was recovered while the symbols are the spectra calculated *in situ* by the processor in the instrument.

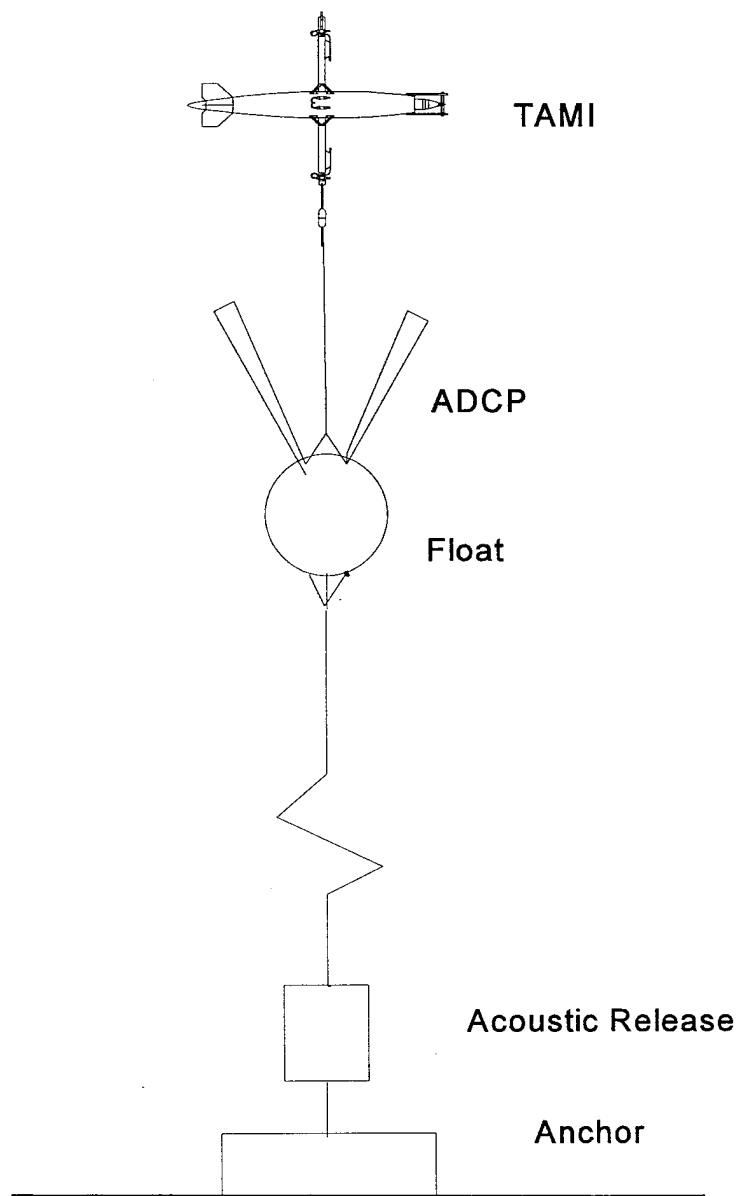7.b   Same as 7.a but for spectra of the signals in figure 6.b.

8. Samples of the normalized spectra of vertical velocity collected at speeds from 0.041 to 0.145 m s^{-1} and progressively offset upwards by one decade for clarity. The flow speed and the rate of dissipation are indicated on the right and left ends of the curves, respectively. Similar results were obtained for the lateral velocity fluctuations.

9. Normalized spectrum of shear in variance preserving form. The shaded region is the 95% confidence limit of the 405 samples using the Bootstrap method (Efron and Gong 1983) while the smooth and thin line is the empirical spectrum after Nasmyth.

10. Spectrum of the output of the analog-to-digital converter on the shear channels for 50 selected cases when the flow was less than 0.01 m s^{-1}, representing the electronic noise of the instrument. The shaded region depicts the 95% confidence interval while the upper and lower lines indicate the maximum and minimum spectral estimate, respectively.

11. Spectra of the electronic noise converted into equivalent shear spectra for speeds ranging from 0.01 to 0.5 m s^{-1} (thin line) versus the expected shear spectrum after Nasmyth for dissipation rates from 10^{-12} to 10^{-6} W kg^{-1}.

12. The estimated rms angle of attack versus flow speed (upper panel) and estimated dissipation rate (lower panel). Values obtained from the w- and v-probes are indicated by "o" and "+", respectively. Few estimates exceed 5°.

13. The estimated rms angle of attack for five increments from 0 to 5° plotted into the ϵU-plane with margins for the electronic noise (solid curve) and the suggested maximum angle of attack of 5° (dashed line). The straight lines indicated the boundaries at 1°, 2°, 3° and 4°.

14. Calibrated sensitivity of the two probes used here versus flow speed.

15. Time series of the rate of dissipation of kinetic energy (upper panel), the Ozmidov or buoyancy length scale (second panel from top), the buoyancy Reynolds number (third panel from top) and the current vector (lower panel) for the deployment in Satellite Channel.
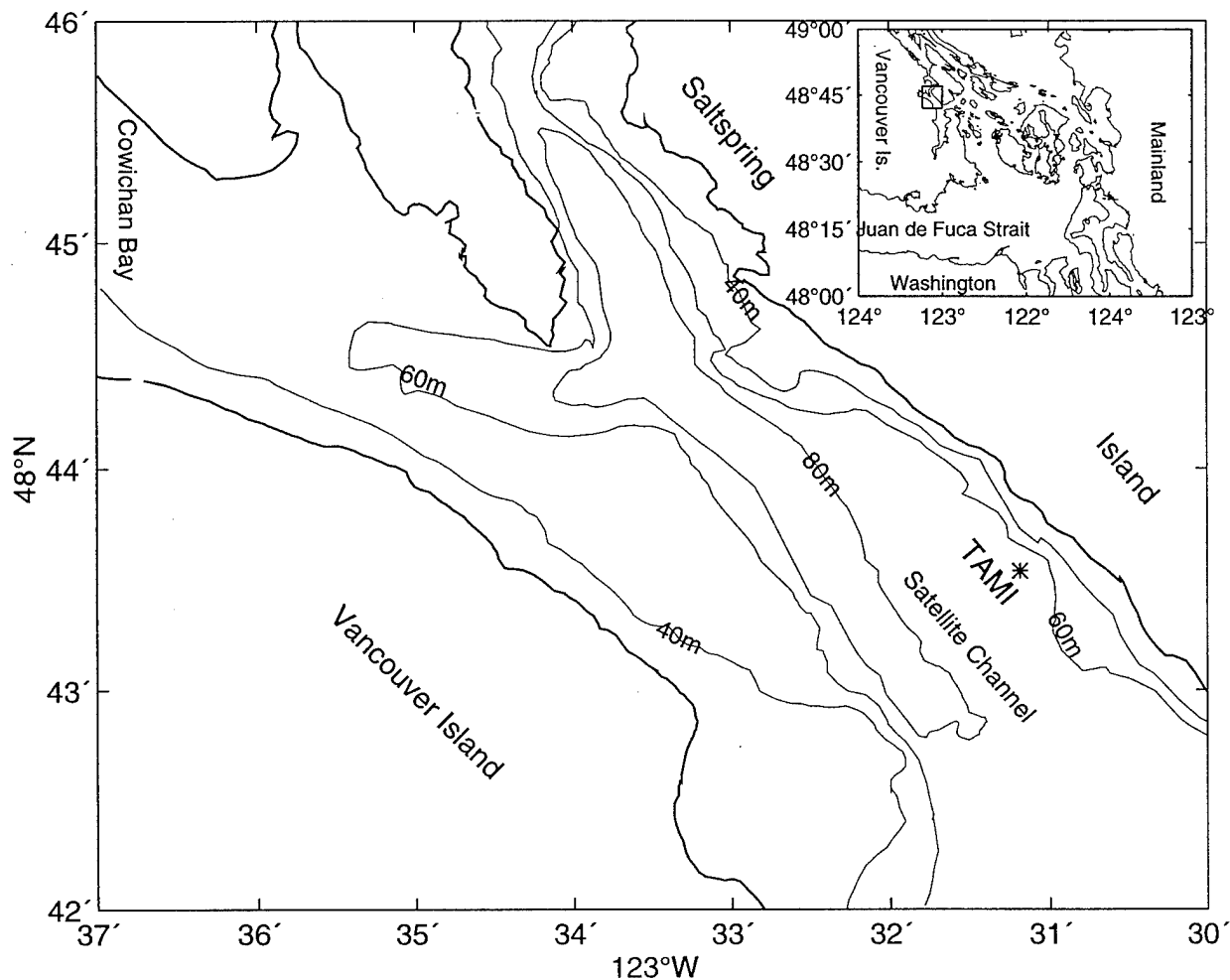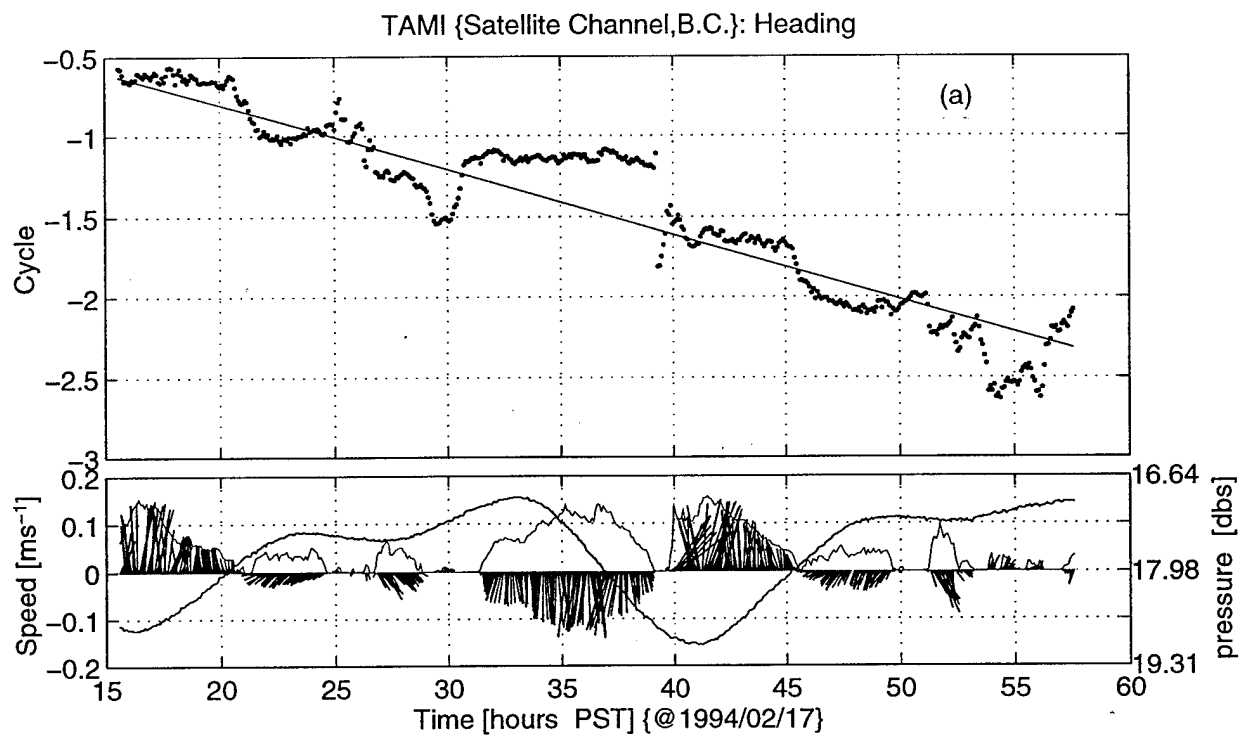
TAMI

Radio & Light Beacons

Conductivity & Temperature Sensors

Current Meter Rotor

Shear Probes & Thermistors

Swivel

1 m

1. Sketch of *TAMI* (*Tethered Autonomous Microstructure Instrument*) which can be anchored using standard techniques and which measures fluctuations of cross-stream velocity and temperature and their horizontal gradients at microscales using shear probes and thermistors. The vertical gradients of conductivity and temperature are measured with three pairs of Seabird sensors. The speed of flow past the instrument is measured with two ducted rotors on the upper and lower masts. The instrument is 5 m long and has a diameter of 0.6 m.

TAMI

ADCP

Float

Acoustic Release

Anchor

2. Typical mooring configuration. The main floatation element is a 1.4 m diameter sphere made of syntactic foam with a buoyancy of 6200 Nt. The line between the acoustic release and the float can be as long as 5000 m. The float also houses and upward looking acoustic doppler current profiler (ADCP). The main instrument, *TAMI*, is 12 m above the float — within the measurement range of the ADCP yet outside the acoustic beams.

Map showing contour lines (40m, 60m, 80m) with labeled features: Cowichan Bay, Saltspring, Vancouver Island, Satellite Channel, Island, and TAMI location (asterisk). Inset map shows Vancouver Is., Mainland, Juan de Fuca Strait, and Washington.

3.   The location of the deployment of *TAMI* on February 17-19 of 1994 (asterisk) in
        Satellite Channel, a minor channel connecting the Georgia Basin to the Pacific Ocean to
        the east of Juan de Fuca Strait.

TAMI {Satellite Channel,B.C.}: Heading

4.a   Time series of heading measured every 5 minutes (dots, upper panel) expressed in cycles. The solid line is the expected rotation for the M_2 tide. The lower panel depicts the current vector (sticks) from the measured speed (thin line) and heading, while the thick line is the pressure.

4.b   Close-up of the heading and current during the change of tide around $t = 39.3$ hours when the flow was weaker than 0.01 m s^{-1} for 40 minutes.
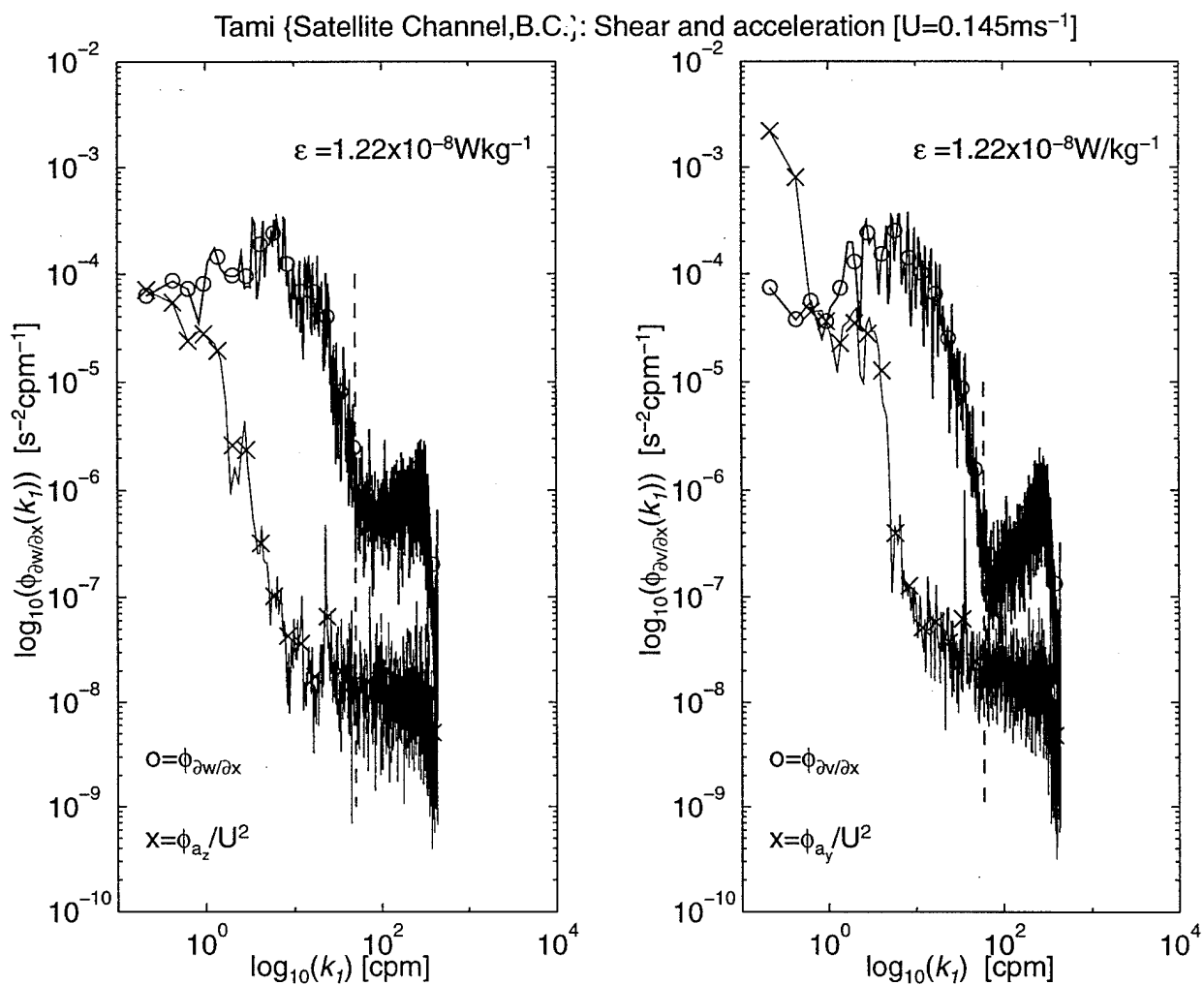
4.c   Close-up of the heading and current during the change of tide around $t = 45.5$ hours when the flow was weaker than 0.01 m s^{-1} for only 10 minutes.

5. Salinity deduced from the top (T), middle (M) and bottom (M) conductivity and temperature sensors (upper panel) along with the current vectors (lower panel). Rapid variations of salinity occur around the change of the tide.

6.a   Unprocessed time series of the shears $\partial w/\partial x$ and $\partial v/\partial x$ recorded by the instrument with full bandwidth (upper two traces, upper panel) and the same shear low-pass filtered at 100 cpm (lower two traces, upper panel) while the flow was 0.145 m s^{-1}. The concurrent full bandwidth acceleration (upper three traces, lower panel) and the accelerations low-pass filtered at 100 cpm (lower three traces, lower panel). The x-acceleration can also be interpreted as pitch for low frequencies (right hand scale) and the y-acceleration as roll. All traces have been offset for clarity.

6.b   Same as for 6.a but for unprocessed data collected during a flow of only 0.045 m s^{-1}.

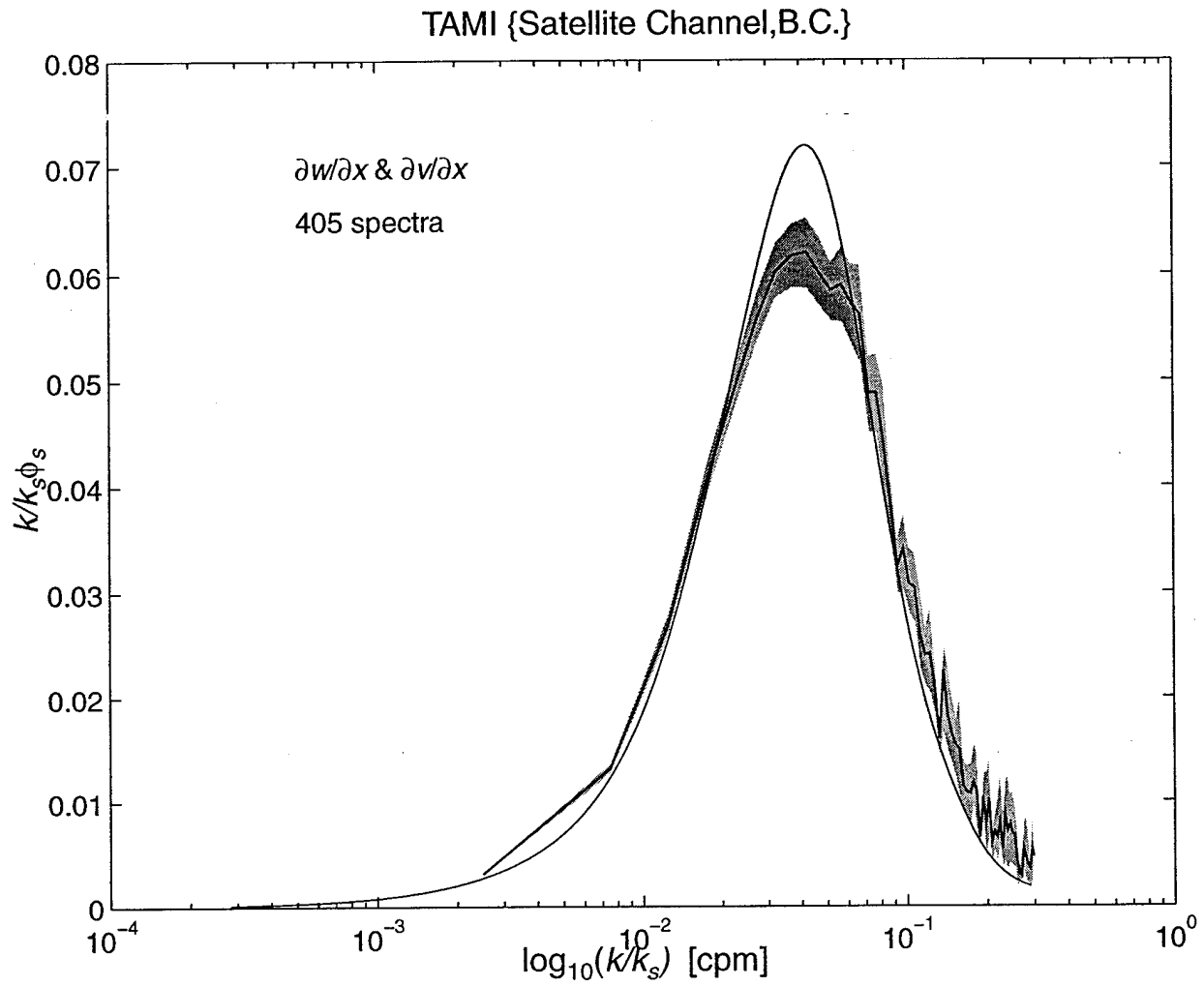Tami {Satellite Channel,B.C.}: Shear and acceleration [U=0.145ms⁻¹]

7.a   Spectra of the shear in figure 6.a with $\partial w/\partial x$ in the left panel and $\partial v/\partial x$ in the right panel. The corresponding acceleration spectra have been scaled by U^{-2} to indicate the contamination due to body vibrations. For the low frequencies, the spectrum of a_y is mainly roll while the spectrum of a_z has a small contribution from pitch and roll. Pitch and roll do not affect the measured shears. The solid lines are the spectra calculated from the unprocessed data after the instrument was recovered while the symbols are the spectra calculated *in situ* by the processor in the instrument.
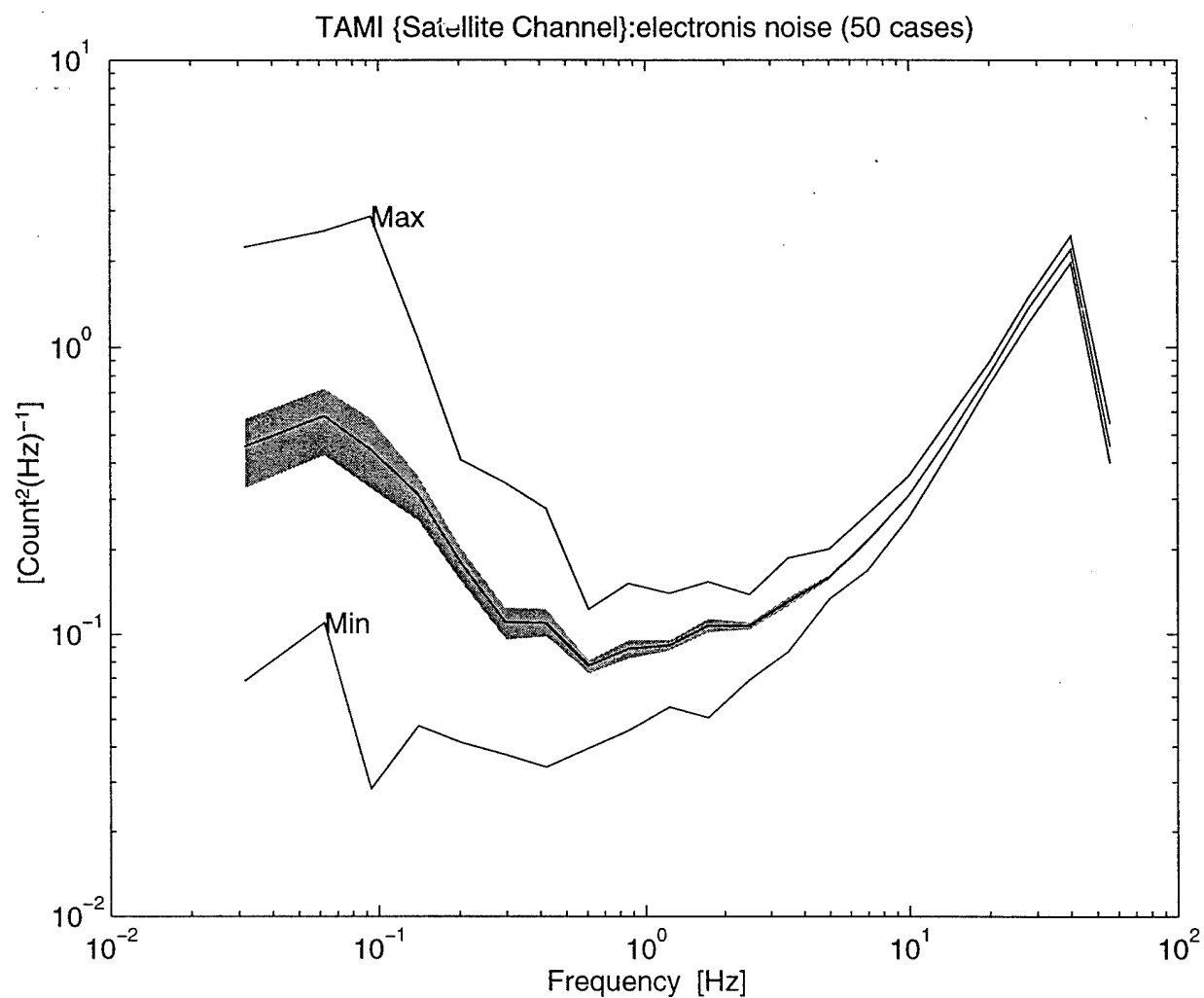
Tami {Satellite Channel,B.C.}: Shear and acceleration [U=0.045ms⁻¹]

7.b   Same as 7.a but for spectra of the signals in figure 6.b.

8. Samples of the normalized spectra of vertical velocity collected at speeds from 0.041 to 0.145 m s^{-1} and progressively offset upwards by one decade for clarity. The flow speed and the rate of dissipation are indicated on the right and left ends of the curves, respectively. Similar results were obtained for the lateral velocity fluctuations.
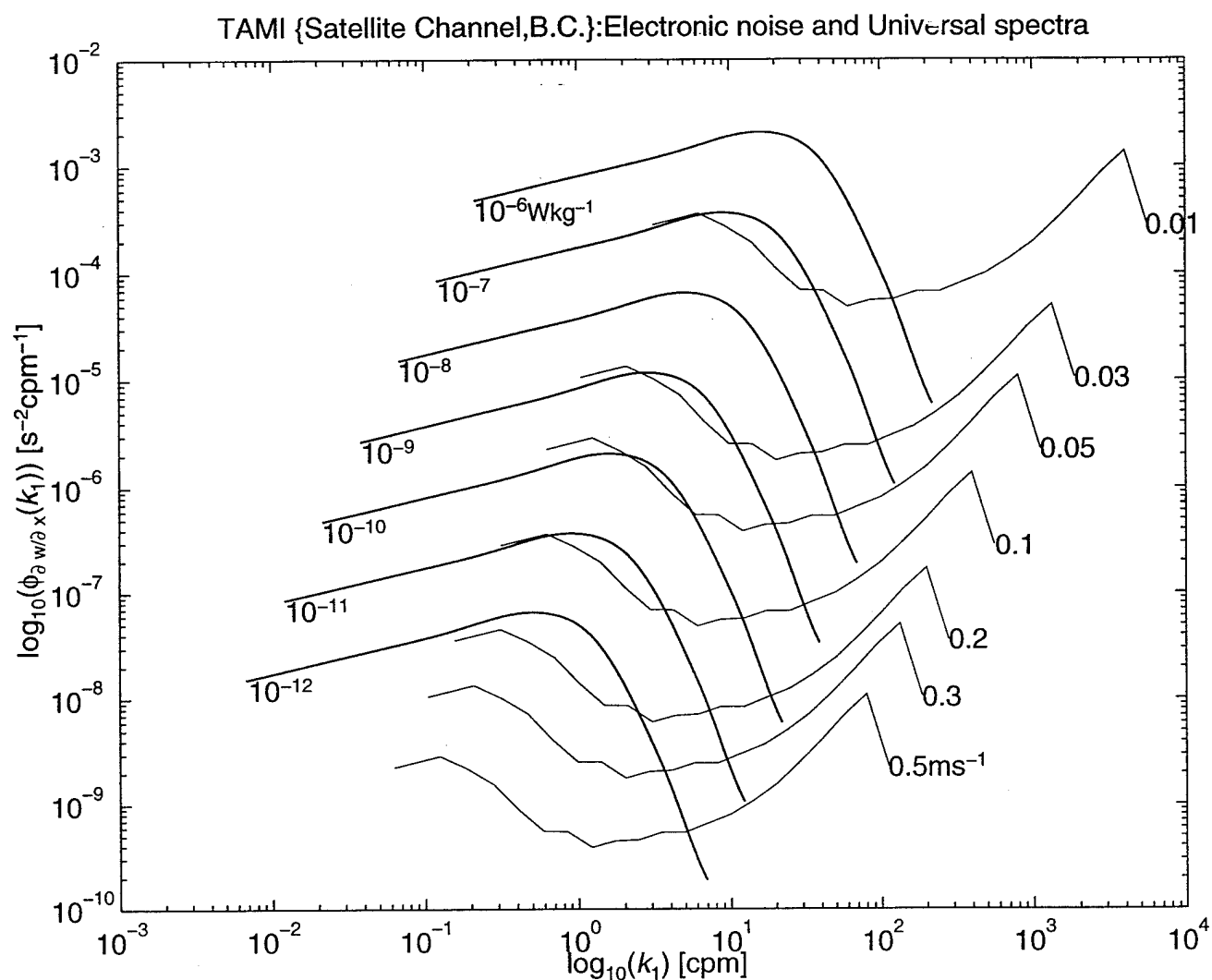
TAMI {Satellite Channel,B.C.}

$\partial w/\partial x$ & $\partial v/\partial x$

405 spectra

y-axis: $k/k_s \phi_s$

x-axis: $\log_{10}(k/k_s)$ [cpm]

9.   Normalized spectrum of shear in variance preserving form. The shaded region is the 95% confidence limit of the 405 samples using the Bootstrap method (Efron and Gong 1983) while the smooth and thin line is the empirical spectrum after Nasmyth.
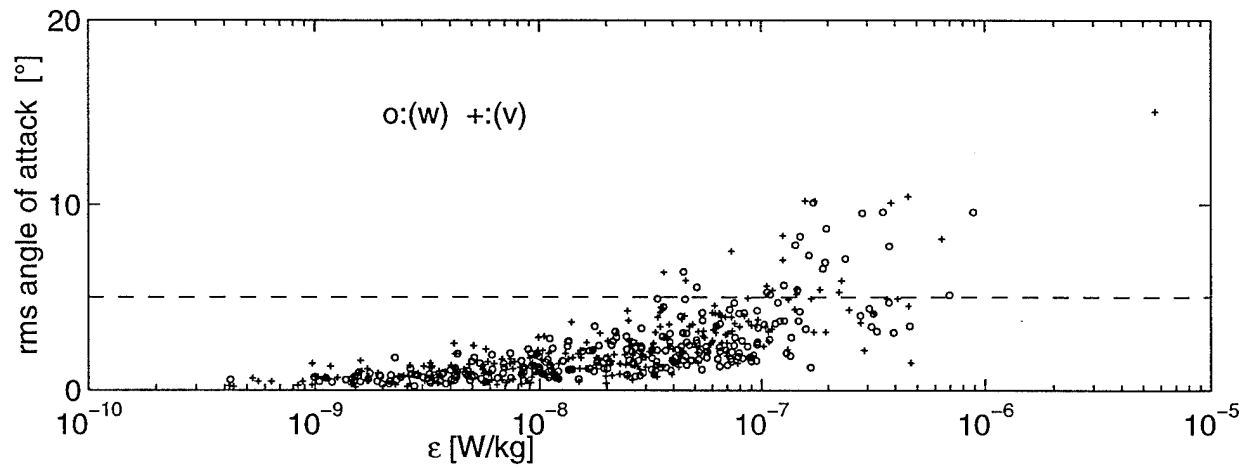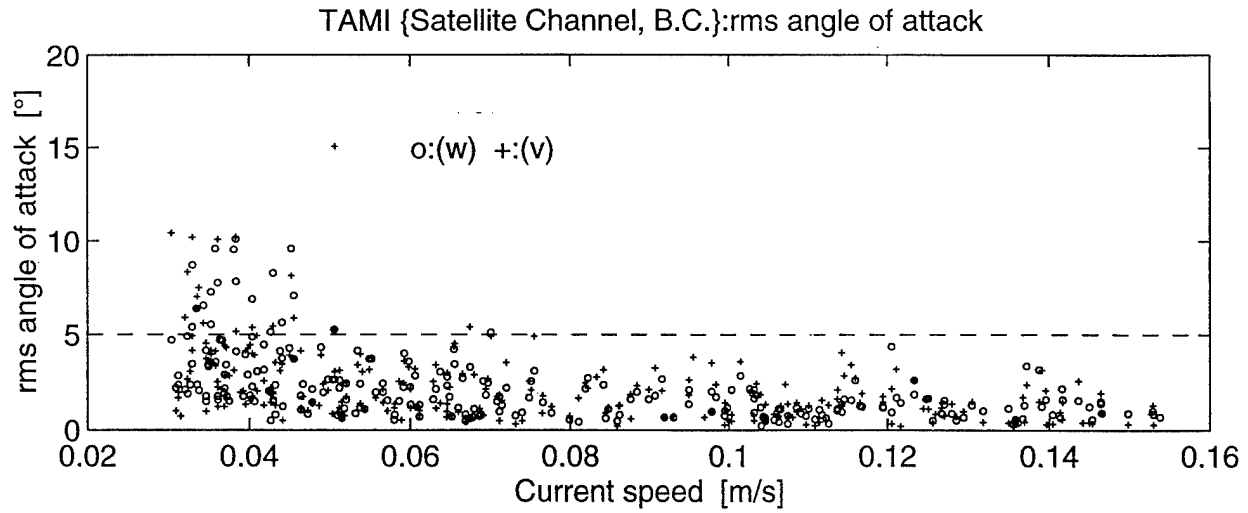
TAMI {Satellite Channel}:electronis noise (50 cases)

10. Spectrum of the output of the analog-to-digital converter on the shear channels for 50 selected cases when the flow was less than 0.01 m s^{-1}, representing the electronic noise of the instrument. The shaded region depicts the 95% confidence interval while the upper and lower lines indicate the maximum and minimum spectral estimate, respectively.
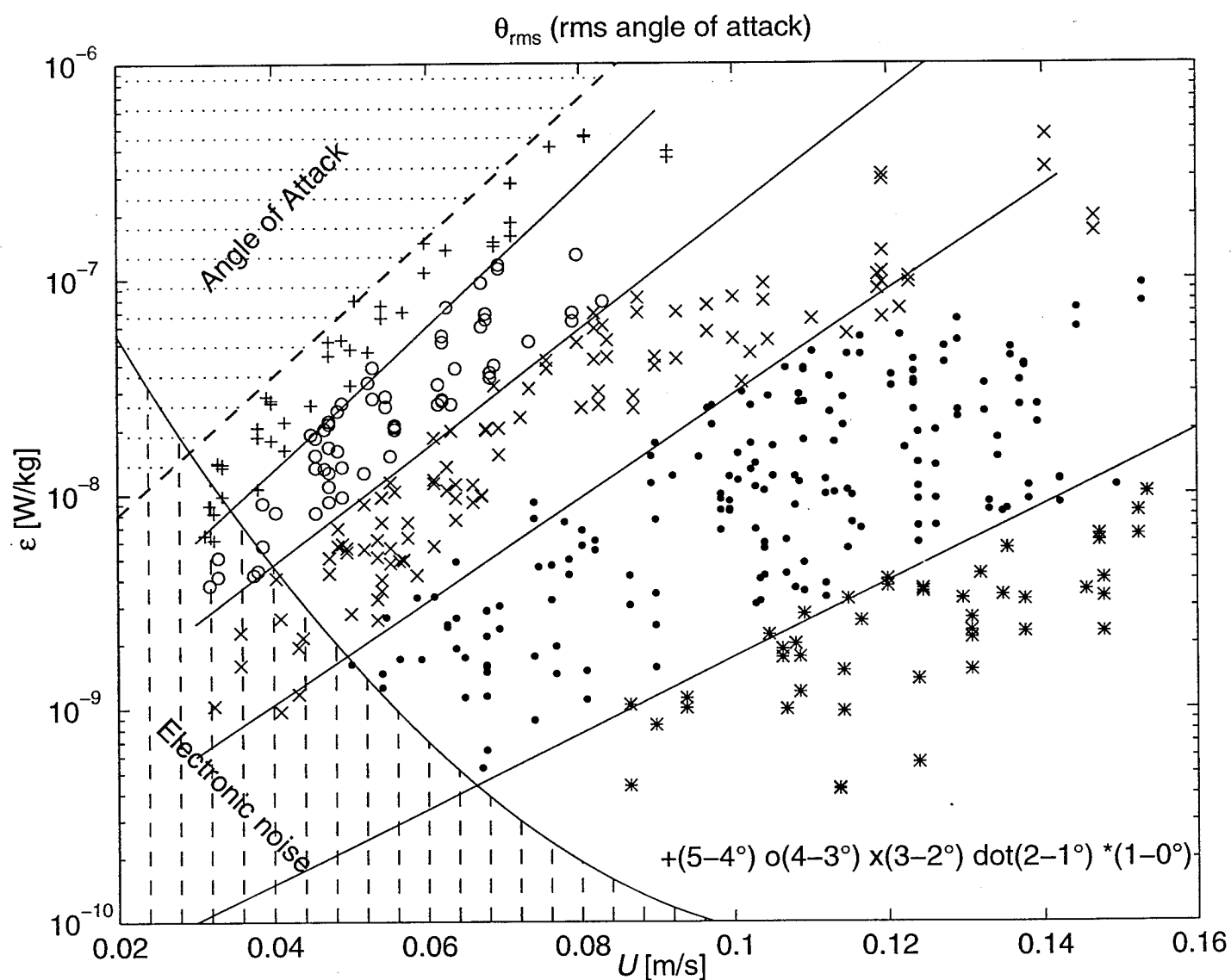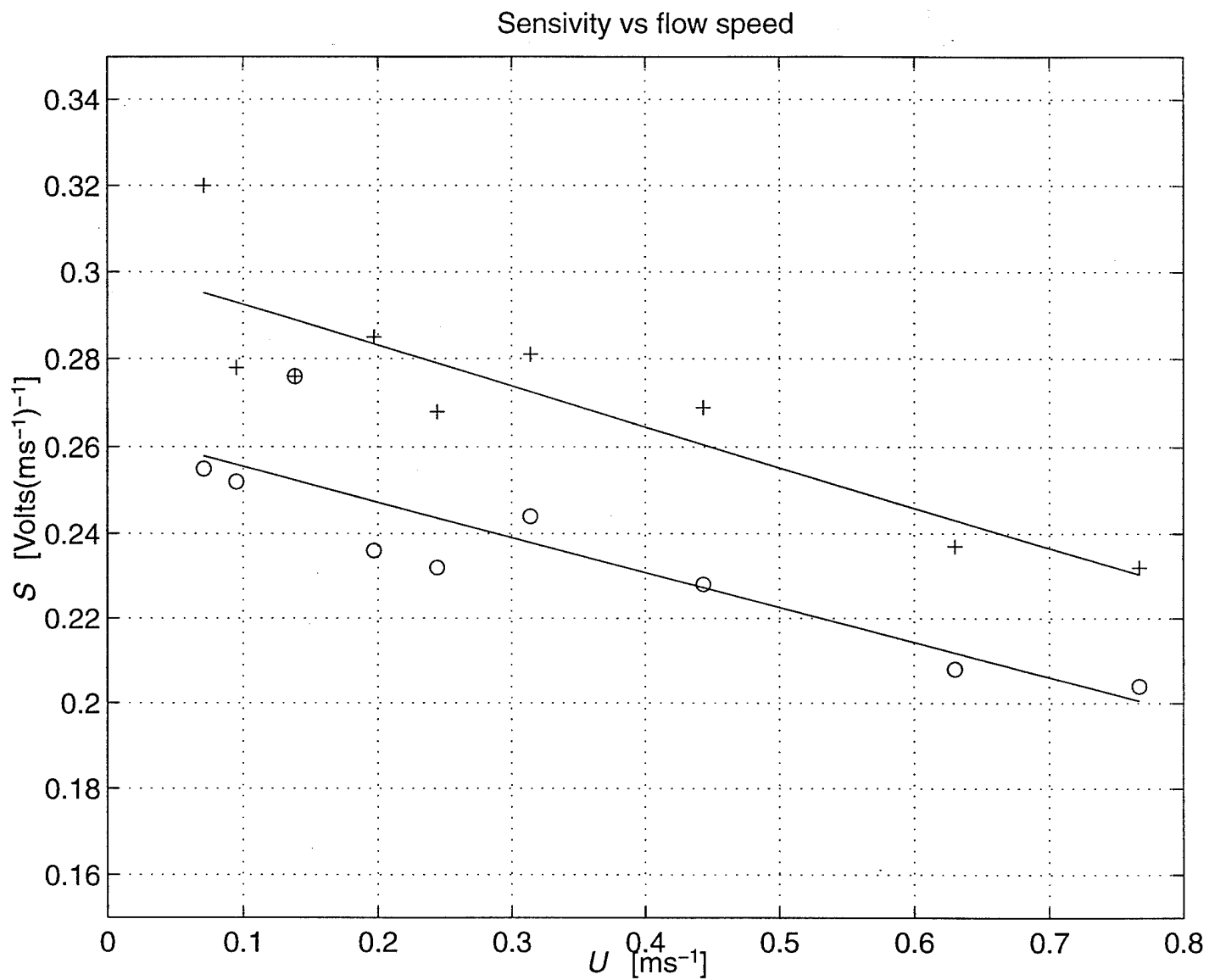
TAMI {Satellite Channel,B.C.}:Electronic noise and Universal spectra

(Vertical axis: $\log_{10}(\phi_{\partial w/\partial x}(k_1))$ $[s^{-2}cpm^{-1}]$)

(Horizontal axis: $\log_{10}(k_1)$ $[cpm]$)

Curve labels (left side): $10^{-6}Wkg^{-1}$, 10^{-7}, 10^{-8}, 10^{-9}, 10^{-10}, 10^{-11}, 10^{-12}

Curve labels (right side): 0.01, 0.03, 0.05, 0.1, 0.2, 0.3, $0.5ms^{-1}$

11. Spectra of the electronic noise converted into equivalent shear spectra for speeds ranging from 0.01 to 0.5 m s^{-1} (thin line) versus the expected shear spectrum after Nasmyth for dissipation rates from 10^{-12} to 10^{-6} W kg^{-1}.
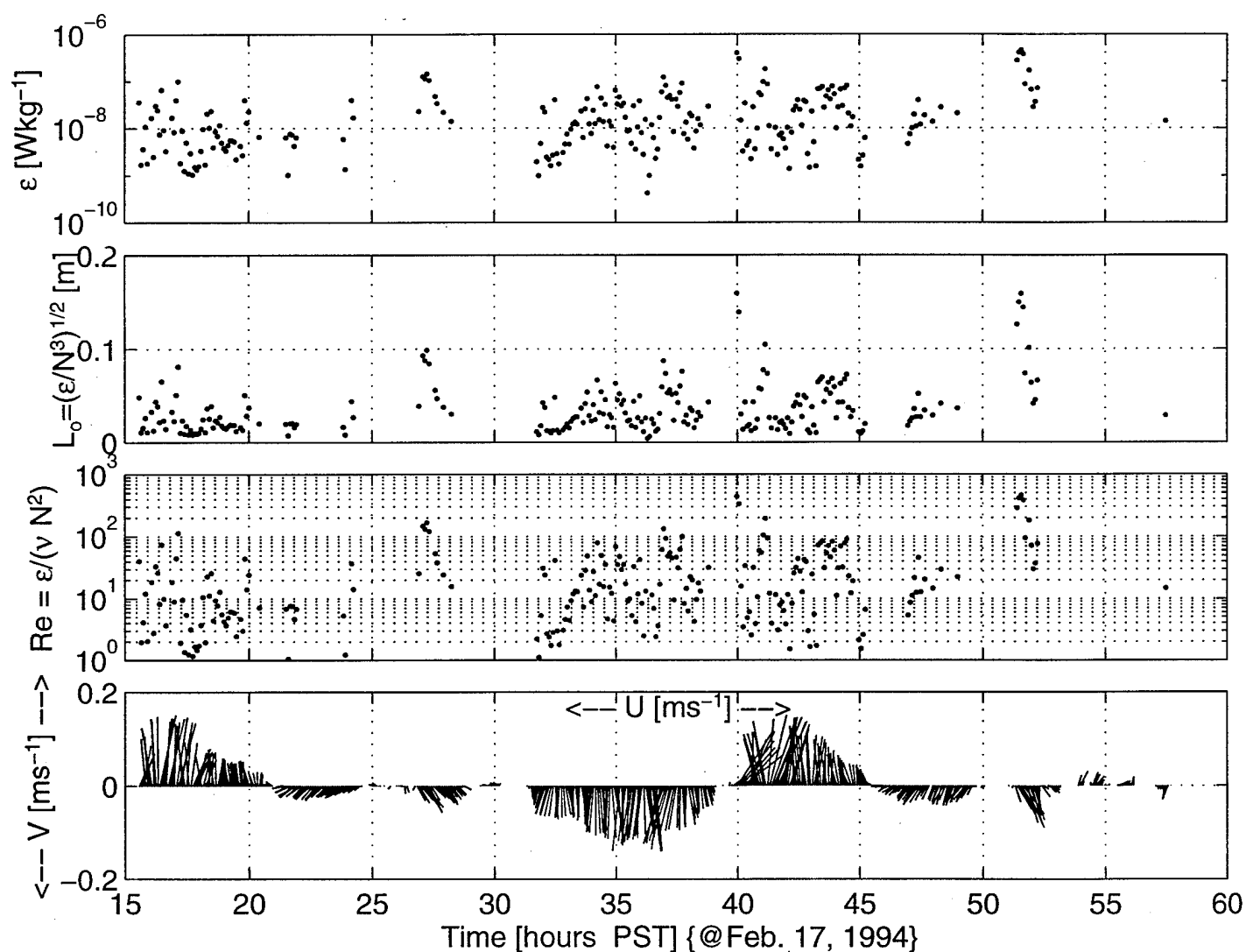
TAMI {Satellite Channel, B.C.}:rms angle of attack

12. The estimated rms angle of attack versus flow speed (upper panel) and estimated dissipation rate (lower panel). Values obtained from the w- and v-probes are indicated by "o" and "+", respectively. Few estimates exceed 5°.

θ_rms (rms angle of attack)

+(5–4°) o(4–3°) x(3–2°) dot(2–1°) *(1–0°)

13. The estimated rms angle of attack for five increments from 0 to 5° plotted into the ϵU-plane with margins for the electronic noise (solid curve) and the suggested maximum angle of attack of 5° (dashed line). The straight lines indicated the boundaries at 1°, 2°, 3° and 4°.

Sensivity vs flow speed

14.   Calibrated sensitivity of the two probes used here versus flow speed.

15.   Time series of the rate of dissipation of kinetic energy (upper panel), the Ozmidov or buoyancy length scale (second panel from top), the buoyancy Reynolds number (third panel from top) and the current vector (lower panel) for the deployment in Satellite Channel.

REPORT DOCUMENTATION PAGE

Public reporting burden for this collection of information is estimated to average 1 hour per response, including the time for reviewing instructions, searching existing data sources, gathering and maintaining the data needed, and completing and reviewing the collection of information. Send comments regarding this burden estimate or any other aspect of this collection of information, including suggestions for reducing this burden, to Washington Headquarters Services, Directorate for Information Operations and Reports, 1215 Jefferson Davis Highway, Suite 1204, Arlington, VA 22202-4302, and to the Office of Management and Budget, Paperwork Reduction Project (0704-0188), Washington, DC 20503.

1. AGENCY USE ONLY *(Leave blank)*	2. REPORT DATE 15 March 1996	3. REPORT TYPE AND DATES COVERED Final: 01 Feb 1991 - 31 Jan 1994

4. TITLE AND SUBTITLE Turbulence Measurements with a Moored Instrument	5. FUNDING NUMBERS G-N00014-91-J-1236

6. AUTHOR(S)

Rolf Lueck

7. PERFORMING ORGANIZATION NAME(S) AND ADDRESS(ES) Centre for Earth and Ocean Research University of Victoria P.O. Box 1700 Victoria, B.C., V8W 2Y2, Canada	8. PERFORMING ORGANIZATION REPORT NUMBER CEOR Report: 96-1

9. SPONSORING / MONITORING AGENCY NAME(S) AND ADDRESS(ES) Department of the Navy Office of Chief of Naval Research 800 Quincy Street, Code 1512 AW Arlington, Virginia, 22217-5000	10. SPONSORING / MONITORING AGENCY REPORT NUMBER

11. SUPPLEMENTARY NOTES

To be published in the Journal of Atmospheric and Oceanic Research

12a. DISTRIBUTION / AVAILABILITY STATEMENT Unlimitted Availability	12b. DISTRIBUTION CODE

13. ABSTRACT *(Maximum 200 words)*

A new, autonomous and moored microstructure measuring instrument has been tested in coastal waters. The instrument measures shear in the dissipation range of the wavenumber spectrum using 4 shear probes, temperature fluctuations using two FP-07 thermistors, temperature and salinity using three pairs of Seabird sensors, horizontal currents using 2 ducted rotors and a fluxgate compass, and body motions using three accelerometers and a pressure transducer. In a two-day experiment, the instrument experienced peak flows of 0.15 m s^{-1} and resolved dissipation rates in currents as slow as 0.03 m s^{-1}. Spectra of velocity fluctuations agree closely with the Nasmyth universal spectrum (Oakey 1982). For dissipation rates, the lower limit of detection is determined by electronic noise while the upper limit is set by the angle of attack of cross-stream velocity fluctuations. Both constraints become less restrictive with increasing current. The electronic noise falls below 10^{-10} W kg^{-1} in flows faster than 0.1 m s^{-1} for which we detected dissipation rates as low as 4×10^{-10} W kg^{-1}. The autonomous instrument makes it possible to obtain long time series at much reduced cost compared to conventional profiling from a ship.

14. SUBJECT TERMS Turbulence, Moored Instrument, Shear Probes, Autonomous Instrument		15. NUMBER OF PAGES 61
		16. PRICE CODE

17. SECURITY CLASSIFICATION OF REPORT UNCLASSIFIED	18. SECURITY CLASSIFICATION OF THIS PAGE UNCLASSIFIED	19. SECURITY CLASSIFICATION OF ABSTRACT UNCLASSIFIED	20. LIMITATION OF ABSTRACT

Standard Form 298 (Rev. 2-89)

GENERAL INSTRUCTIONS FOR COMPLETING SF 298

The Report Documentation Page (RDP) is used in announcing and cataloging reports. It is important that this information be consistent with the rest of the report, particularly the cover and title page. Instructions for filling in each block of the form follow. It is important to *stay within the lines* to meet *optical scanning requirements*.

Block 1. Agency Use Only *(Leave blank)*.

Block 2. Report Date. Full publication date including day, month, and year, if available (e.g. 1 Jan 88). Must cite at least the year.

Block 3. Type of Report and Dates Covered. State whether report is interim, final, etc. If applicable, enter inclusive report dates (e.g. 10 Jun 87 - 30 Jun 88).

Block 4. Title and Subtitle. A title is taken from the part of the report that provides the most meaningful and complete information. When a report is prepared in more than one volume, repeat the primary title, add volume number, and include subtitle for the specific volume. On classified documents enter the title classification in parentheses.

Block 5. Funding Numbers. To include contract and grant numbers; may include program element number(s), project number(s), task number(s), and work unit number(s). Use the following labels:

C	-	Contract	PR -	Project
G	-	Grant	TA -	Task
PE	-	Program Element	WU -	Work Unit Accession No.

Block 6. Author(s). Name(s) of person(s) responsible for writing the report, performing the research, or credited with the content of the report. If editor or compiler, this should follow the name(s).

Block 7. Performing Organization Name(s) and Address(es). Self-explanatory.

Block 8. Performing Organization Report Number. Enter the unique alphanumeric report number(s) assigned by the organization performing the report.

Block 9. Sponsoring/Monitoring Agency Name(s) and Address(es). Self-explanatory.

Block 10. Sponsoring/Monitoring Agency Report Number.

Block 11. Supplementary Notes.

Block 12a. Distribution/Availability Statement. Denotes public availability or limitations. Cite any availability to the public. Enter additional limitations or special markings in all capitals (e.g. NOFORN, REL, ITAR).

DOD - See DoDD 5230.24, "Distribution Statements on Technical Documents."
DOE - See authorities.
NASA - See Handbook NHB 2200.2.
NTIS - Leave blank.

Block 12b. Distribution Code.

DOD - Leave blank.
DOE - Enter DOE distribution categories from the Standard Distribution for Unclassified Scientific and Technical Reports.
NASA - Leave blank.
NTIS - Leave blank.

Block 13. Abstract. Include a brief *(Maximum 200 words)* factual summary of the most significant information contained in the report.

Block 14. Subject Terms. Keywords or phrases identifying major subjects in the report.

Block 15. Number of Pages. Enter the total number of pages.

Block 16. Price Code. Enter appropriate price code *(NTIS only)*.

Blocks 17. - 19. Security Classifications. Self-explanatory. Enter U.S. Security Classification in accordance with U.S. Security Regulations (i.e., UNCLASSIFIED). If form contains classified information, stamp classification on the top and bottom of the page.

Block 20. Limitation of Abstract. This block must be completed to assign a limitation to the abstract. Enter either UL (unlimited) or SAR (same as report). An entry in this block is necessary if the abstract is to be limited. If blank, the abstract is assumed to be unlimited.